Title	Controlled assembly of metal nanostructures and their application to sensitive molecular sensing(Dissertation_)
Author(s)	Matsuoka, Tomoyo
Citation	Kyoto University ( )
Issue Date	2013-03-25
URL	http://dx.doi.org/10.14989/doctor.k17583
Right	
Type	Thesis or Dissertation
Textversion	author

Controlled assembly of metal nanostructures and their application to sensitive molecular sensing

Tomoyo   Matsuoka

2013

Contents

General Introduction

Gold nanoparticles have received great interests due to the attractive electronic, optical, chemical, and thermal properties as well as catalytic properties and potential applications in the fields of physics, chemistry and material science [1]. Since they are the most chemically stable among metal nanoparticles and have lower toxicity (biocompatibility) compared to other noble metals, they have also attracted considerable attentions in biological and medical fields. Their unique physical properties are provided by the nanoscopic dimension, and are often completely different from those observed for bulk gold. Synthesis of citrate stabilized gold nanoparticles was first reported in the 1950's by Turkevich et al. [2] and in the 1970's by Frens [3]. An important breakthrough was made by Brust et al. in 1994 [4], who developed a synthetic strategy yielding smaller gold nanoparticles with a relatively narrow size distribution and a stabilizing self-assembled monolayer of thiols. The size of the nanoparticles can be tuned by varying the gold to ligand ratio in the synthesis, where a larger amount of ligand leads to smaller particles. Since then, gold nanoparticles have been the subject of a considerably increased number of books and reviews. Various applications have been proposed and some of them have already been realized by utilizing the synthesized nanoparticles with finely controlled morphology.

Most of the prominent properties of gold nanoparticles arise from their surface plasmon resonance. When a small metal nanoparticle is irradiated by light, the

oscillating electric field causes the conduction electrons to oscillate coherently, which is called the surface plasmon resonance, and leads to the enhancement of the local electromagnetic field [5]. Not only does the surface plasmon give rise to the intense colors of suspensions or sols containing the nanoparticles, it has been used to enhance the surface sensitivity of several spectroscopic measurements including fluorescence, second harmonic generation and Raman scattering [6]. The strong coupling between light and surface plasmon in nanoparticles also leads to novel phenomena such as optical force enhancement in nanoaggregates, transport and storage of energy, as well as controlling the anisotropic growth of nanoparticles, and measuring intramolecular and conformational distances in molecules. Generally, the plasmon frequency of the electrons is determined by four factors; the size and shape of the charge distribution, the density of electrons and the effective electron mass. Tuning of the frequency can be achieved by controlling the size, shape and environment for each metal depending on experimental or practical requirements [7]. Recent advances in synthesizing techniques to fabricate nanoparticles with a specific size and shape enable us to tailor surface plasmon properties for clearly defined applications. Gold nanoparticles are easy to synthesize and typically have plasmon frequencies located from visible to near infrared (NIR) wavelength, which makes

them particularly suitable as building blocks of plasmon devices which work with

widely-used laser sources such as Nd:YAG, Nd:YVO4 or He-Ne laser.
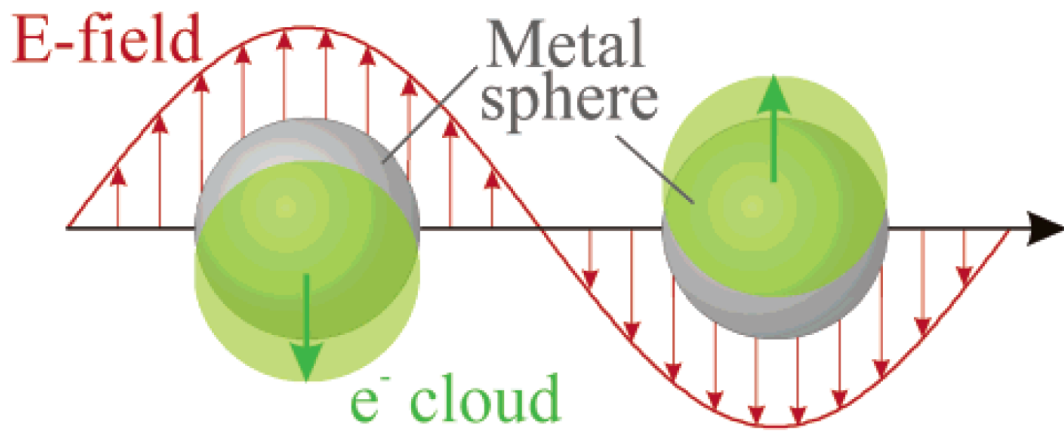
Figure 1. Schematic of plasmon oscillation (from Ref. 5)

The synthesis strategy for the nanoparticles with various sizes and shapes span a wide range of procedures. The synthesis of spherical nanoparticles has been exhaustively studied, and several well established methods are available. The synthesis of anisotropic nanoparticles can be achieved by selective adsorption of capping agents such as cetyltrimethylammonium bromide (CTAB) [8] and several other selective adsorbates which direct the growth process.

In order to integrate these synthesized particles into devices, it is then required to organize or assemble them onto substrates. Substantial efforts have been devoted to organizing nanoparticles in one, two and three dimensions. There are generally two approaches in patterning and controlling spatial assembly of nanoparticles; "bottom-up" (e.g., self-assembly) and "top-down" (e.g., lithographic techniques) approaches. In bottom-up approach, attachments via either covalent or electrostatic interaction between nanoparticle and substrate are widely used. Self-assemblies of nanoparticles onto solid surfaces based on interaction using polymers and biomolecules have also been widely reported [9]. On the other hand, in top-down approach, focused ion beam (FIB) milling and electron-beam lithography (EBL) have been widely used [10], both of which allow fine control over the size and shape of nanostructures. Incorporation of these two approaches is also growing field and have provided new directions for the creation of functional materials and devices. Although various techniques have already been developed for fabrication of electronic or optical devices using gold nanoparticles [11], most of them are time-consuming and lack versatility. It is, therefore, still needed to

develop a simple and versatile technique which can practically be applied to fabrication of these devices in order to fully utilize unique and superior properties of gold nanoparticles.

Among numerous applications utilizing prominent properties of gold nanoparticles, Surface Enhanced Raman Scattering (SERS) is one of the most popular subjects[6] [12] [13]. SERS has been considered as highly useful technique resulting in strongly increased Raman signals from molecules which have been attached to nanometer sized metallic structures. Normal Raman scattering of a molecule is inherently weak due to the small Raman cross-section that is nearly 14 orders of magnitude lower than those of fluorescence emission. With SERS effect, however, the signal intensity can be enhanced more than 15 order of magnitude, which make Raman signal comparable or even superior to fluorescence. It is generally agreed that more than one effect contributes to the observed large effective SERS cross section. The enhancement mechanisms are roughly divided into electromagnetic and chemical effects. The electromagnetic enhancement arises from enhanced optical fields due to excitation of electromagnetic resonances in the metallic structures.

The present work was first motivated by an incidentally-observed phenomenon, in which gold nanoparticles were found to assemble in line on surface of unprocessed silicon substrate when I tried to observe synthesized gold particles. Since the detailed investigation of the phenomenon indicated the possibility to apply it to a simple technique for gold nanopatterning on silicon substrate, my first work focused on
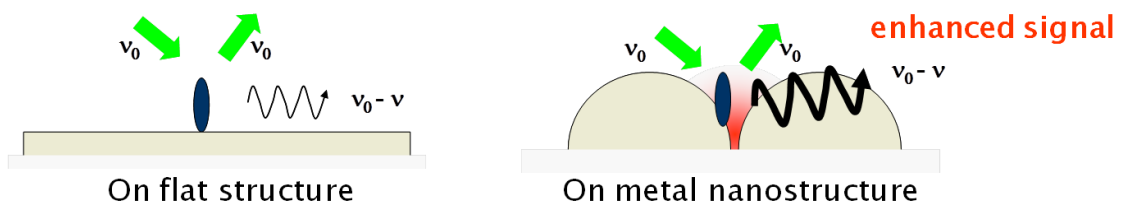
Figure 2. Schematic representation of surface enhanced Raman scattering.

developing the patterning technique using FIB and femtosecond laser. The technique is unique in that the gold nanopatterning is based on selective precipitation of gold on FIB- or laser- processed areas, that is, it is achieved by combining both bottom-up and top-down approaches. In addition to the development, I have worked on fabrication of SERS-active substrates using the developed patterning technique. Since the technique is only available for silicon substrate, as the next step to utilize SERS-activity of gold nanoparticles, I have also worked on making the surface of transparent polymer material SERS-active by functionalizing them with gold nanoparticles. The technique uses silica xerogel to immobilize gold nanoparticles on polymer surface (SU-8) and was found to be useful in functionalizing the surface of SU-8 with various materials such as environmentally-responsive fluorescent molecules. The contents of respective chapters are summarized as follows.

In chapter 1, maskless and electroless patterning of gold was performed by a simple method: 3-mercaptopropyltrimethoxysilane (MPTMS) and an aqueous solution of hydrogen tetrachloroaurate ($HAuCl_4 \cdot 4H_2O$) were reacted, and the obtained solution was dropped onto a silicon substrate processed by an FIB. This method utilizes the selective growth of gold nanoparticles on an FIB-processed area of a silicon surface. Raman microspectroscopy revealed that gold nanoparticles selectively grew on an FIB-processed area when an amorphous silicon phase was induced by an FIB.

In chapter 2, I demonstrated that gold patterning on silicon substrate can also be performed with the assistance of femtosecond laser. Gold precipitation with high

density can be achieved only when amorphous silicon phase was induced, as indicated in chapter 1 using an FIB. The results imply that any processing tools can be used for this patterning method as long as it can induce amorphous silicon phase. I can select the most suitable tool from among three (FIB, laser and AFM) in accordance with the purpose or requirements.

In chapter 3, I applied our metal patterning method to facile fabrication for SERS-active substrate. Both gold and silver structures showed reasonable SERS enhancement and I found that there is an optimal size of particles determined by dielectric constant of the metal and the wavelength used for excitation. Since the size and the aggregation degree of the metal structures can be easily controlled by varying experimental conditions such as reaction temperature, reaction time and concentration of the metal ion solution, we can optimize the structure depending on which laser is available and which metal is more suitable for analytes to be sensed.

In chapter 4, I have functionalized surfaces of photopolymerized SU-8 by coating them with silica-based xerogel prepared with a fluorescent calcium indicator or gold nanoparticle. The results show that these materials are entrapped inside the gels and retain the responsiveness. I have confirmed that the heat treatment after spin coating is effective in improving adhesion and hardness of the obtained films, which is mainly associated with the Si-O-C bond formation at the interface due to the enough amounts of Si-OH and epoxy group remained in the reaction system. I have also demonstrated that the method can be applied to local coating of microstructures, which expands

possibilities for fabrication of micro-systems such as MEMS sensors or micro-TAS (total analysis system) devices based on SU-8.

References

[1]   M.C. Daniel and D. Astruc Chem. Rev. **104** (2004), 293.

[2]   J. Turkevich, P.C. Stevenson and J. Hillier, Discuss Faraday Soc **11** (1951), 55.

[3]   G. Frens, Nature Physical Science **241** (1973), 20.

[4]   M. Brust, M. Walker, D. Bethell, D.J. Schiffrin and R. Whyman, J Chem Soc Chem Commun **7** (1994), 801

[5]   K. L. Kelly, E. Coronado, L. L. Zhao and G. C. Schatz, J. Phys. Chem. B **107** (2003), 668

[6]   P. L. Stiles, J. A. Dieringer, N. C. Shah and R. P. V. Duyne, Annual Review of Analytical Chemistry **1** (2008), 601

[7]   C. Noguez, J. Phys. Chem. C **111** (2007), 3806

[8]   C. J. Murphy, T. K. Sau, A. M. Gole, C. J. Orendorff, J. Gao, L. Gou, S. E. Hunyadi and T. Li, J. Phys. Chem. B **109** (2005), 13857

[9]   Y. Ofir, B. Samanta and V. M. Rotello, Chem. Soc. Rev. **37** (2008), 1814

[10]   M. Kahl, E. Voges, S. Kostrewa, C. Viets and W. Hill, Sensors and Actuators B-Chemical **51** (1998), 285

[11]   M. Fana, G. F.S. Andradec and A. G. Brolo, Analytica Chimica Acta **693** (2011), 7

[12]   K. Kneipp, Y. Wang, H. Kneipp, L. T. Perelman, I. Itzkan, R. R. Dasari, and M. S. Feld, Phys. Rev. Lett. **78** (1997), 1667

[13] E. C. Le Ru, E. Blackie, M. Meyer, and P. G. Etchegoin, J. Phys. Chem. C **111** (2007), 13794

Chapter 1

Selective growth of gold nanoparticles on FIB-induced amorphous phase of Si substrate

1.1 Introduction

Metal patterning on a silicon surface has wide range of applications in electronics fields: Schottky diodes [1], integrated circuits (IC) [2], [3], through holes for printed boards [4], and so on. The patterning is attracting increased attention because it can also be applied to wire grid polarizers for terahertz waves [5], and to surface plasmon resonance devices [6]. Several types of metal-patterning methods have been reported in the past. The most common and well-known methods are photolithography for micropatterning and electron-beam lithography for nanopatterning. Both techniques are, however, indirect approaches and many steps are needed to obtain the target metal structures: coat Si substrate with resist film, modify parts of resist film using UV light (with masking) or an electron beam, remove either modified or unmodified part selectively, deposit metal on substrate, and finally remove residual resist. In this final step, the metal structures deposited on the residual resist are removed together with the resist so that only the metal structures deposited directly on the Si surface are left. Methods for fabricating metal structures more easily by direct modifying of the Si surface (i.e., resistless and

12

maskless processes) have thus been attracting much attention recently. Electrodeposition

process is commonly involved in this approach [7]. This method utilizes high reactivity

of the modified parts of Si surface for electrodeposition. Homma et al. reported a direct

and electroless process [8] in which the surface of a hydrogen-terminated P-type Si wafer

is directly modified by nanoindentation and then immersed into aqueous solution of

$Cu(NO_3)_2$ and HF. Copper nanostructures selectively form at the nanoscopic defect sites,

that is, the nanoindentation locations. I previously reported a simple method for

preparing single crystalline tabular gold microparticles with nanoscale thickness. An

ethanol solution of 3-mercaptopropyltrimethoxysilane (MPTMS) is mixed with an

aqueous solution of hydrogen tetrachloroaurate $(HAuCl_4 \cdot 4H_2O)$ [9]. Observation of the

reaction products on an undoped Si wafer (single-sided; cut in pieces of 1 cm^2) using a

field-emission scanning electron microscope (FE-SEM) revealed one-dimensional (1D)

arrays of gold nanoparticles (with approximately 10 nm in diameter) in addition to gold

microplates. It was found that possibility of 1D arrays depends on the way to snap Si

wafer off: the possibility is higher in snapping so that the polished surface is inside than

in snapping so that the polished surface is outside. This phenomenon implied that the

1D arrays of gold nanoparticles were formed on the local active sites induced by stress

generated by snapping. It was also found that gold nanoparticles selectively precipitate

on the surface scratched intentionally and weakly by hand with a diamond pencil, but do

not precipitate on that scratched strongly. This implies that there is an optimum stress

for inducing active sites for arrays of gold nanoparticles. Here, I have used a focused

ion beam (FIB) to perform nano/micro processing and developed a direct and electroless method for gold patterning on a Si surface. In this work, the solution dropped on to the FIB-processed Si wafer was adjusted to grow only spherical nanoparticles on the FIB-processed area, which enabled us to inhibit the formation of tabular microparticles that were unfit for our purpose.

1.2 Experimental

Our method for gold patterning consists of three steps, as shown in Fig. 1. Undoped Si (100) wafers, which were precleaned by sonication for 5 minutes in ethanol, were used. Geometric patterns were written on them with a Ga FIB (JEM-9310, JEOL, Japan) at 30 kV. A drop of prepared suspension was then dropped on the wafer, and the wafers were dried at 80 °C. The suspension contained a mixture of 42.5 μl of MPTMS and 3 ml of 0.05 M aqueous solution of $HAuCl_4$ and was prepared by stirring on a hot plate set to 100 °C for 2 hours. A Raman microspectrometer (Nanofinder30, Tokyo Instruments, Japan; wavelength = 532 nm, NA = 0.6), a FE-SEM (JSM6700F, JEOL, Japan), and an energy dispersive X-ray spectrometer (JED-2300, JEOL, Japan) were used to investigate the processed wafers and gold nanostructures. Table 1 shows the relationship between the irradiation current and the beam width for the ten beams available with the FIB (JEM-9310). I chose beams: 2, 8, and 9 (this selection of beams has no special significance). To obtain an FIB-processed area large enough for Raman analysis, I processed the Si substrate using only the beam effect caused while scanning ion

microscope (SIM) image is obtained (beam 2 for 30 seconds).

1.3 Results

Figure 2 shows a SEM image of a sample obtained using the beam with an irradiation current (IC) of 50 pA, a beam width (BW) of 20 nm, and an estimated dosage (ED) of 6.2×10^{16} ions/cm^2. Figure 3 shows the result of energy dispersive X-ray spectrometer (EDS) line profile analysis for Au. As can be seen, the fabrication of gold patterns with high spatial selectivity was achieved. Raman spectra for the FIB-processed and unprocessed areas are shown in Fig. 4 and 5. The spectrum for the processed area (Fig. 4) differed from that for the unprocessed area (Fig. 5) and showed not only the peaks of crystalline silicon (known as Si-I) but also two other peaks (broad peaks at 470 and 150 cm^{-1}), which can be assigned as amorphous silicon. This phenomenon (i.e., the transition of crystalline silicon to amorphous silicon due to FIB irradiation) was also reported by Rubanov and Munroe [10]. To investigate the importance of amorphous silicon in gold precipitation, a part of FIB-processed area was recrystallized and the procedure for gold precipitation was performed. Recrystallization of amorphous silicon was achieved by irradiation of tightly focused laser beam. The beam from an Nd:YAG CW laser with a wavelength of 532 nm can produce crystalline silicon phase from amorphous silicon [11]. The numerical aperture (NA) of the objective lens used for this was 0.9, which is larger than that of the lens used for Raman analysis (NA = 0.6). Figure 6(a) shows a SEM image of a laser irradiated area on amorphous silicon induced by an

FIB. The Raman spectrum of this area (Fig. 6(b)) indicates that the amorphous silicon was recrystallized by the laser irradiation. Figure 6(c) shows a backscattered electron image of the same area as Fig. 6(a) but was captured after gold precipitation. Gold nanoparticles were observed on the FIB-processed area (i.e., amorphous silicon area) but almost no gold nanoparticles in the laser-irradiated area (i.e., the recrystallized area). Figure 7 shows FE-SEM images of the gold structures for three FIB-processing times (i.e., dosages) created using beam 9 (IC = 10 pA, BW = 15 nm); (a) 1.2×10^{16}, (b) 1.2×10^{17}, and (c) 3.75×10^{17} ions/cm^2. These results indicate that, in this range of dosage, increasing the dosage increases the amount of gold structures.

1.4 Discussion

The results in Figs. 4, 5 and 6 show that the amorphous phase plays an important role on the fabrication of gold nanostructures on silicon. The importance of the induced amorphous phase was also demonstrated by our results for scratching with a diamond pencil: I obtained 1D gold nanoparticle arrays on lines scratched by hand weakly with a diamond pencil but not on ones scratched strongly. In the same way as FIB, I have also confirmed using Raman microspectroscopy that the amorphous silicon phase was dominant in the area scratched weakly whereas little amorphous phase in the area scratched strongly (the data is not shown here). Similar phenomenon was reported by R. Gassilloud et al. [12]. Why is the amorphous phase important? Dangling bond defects may be an origin, because it is well known that commercially available amorphous

16

silicon is intentionally terminated by hydrogen. I can expect that amorphous silicon induced by an FIB has a large number of active sites compared with crystalline silicon. Since the number of the active sites decreases considerably by laser annealing, it is difficult for gold to precipitate on the annealed area as shown in Fig. 6. The amorphization and damage level of ion-irradiated crystalline silicon have been investigated by other groups and they showed threshold-like increase in damage with increasing dosage [13]. This dependence of the damage on ion dosage is similar to the dependence of the number of precipitated gold nanoparticles on dosage in Fig. 7. Thus, significant contribution of the induced defects to the selective growth of gold nanoparticles is implied. In our previous works, MPTMS worked as a reducing agent and produced gold particles in the solution containing aurate (III) ions [9]. In this work, I modulated the reaction conditions of MPTMS and aurate ion. This modulation resulted in a partial and incomplete reduction of aurate (III) ions: a large number of gold particles were identified after keeping the solution at 80 °C for 24 h, whereas no change was observed when it was kept at room temperature. It is also noted that $HAuCl_4$ aqueous solution did not give us the gold pattern without MPTMS. I expect that partially reduced aurate ions can be completely reduced to gold nanoparticles once further energy or electrons are given from active sites of the FIB-processed area.


1.5 Conclusions

I applied our previous synthesizing method to fabricating patterned gold

17

nanostructures on silicon wafer. Using FIB irradiation, I obtained gold patterns about 300 nm wide with high spatial selectivity. The fabricating process is very simple, and the overall process is maskless and electroless. This means that its use should reduce costs and open the door to new applications. I also demonstrated that the presence of amorphous silicon is important for fabricating gold nanostructures.

Table 1. Relationship between irradiation current and beam width
for ten beams available

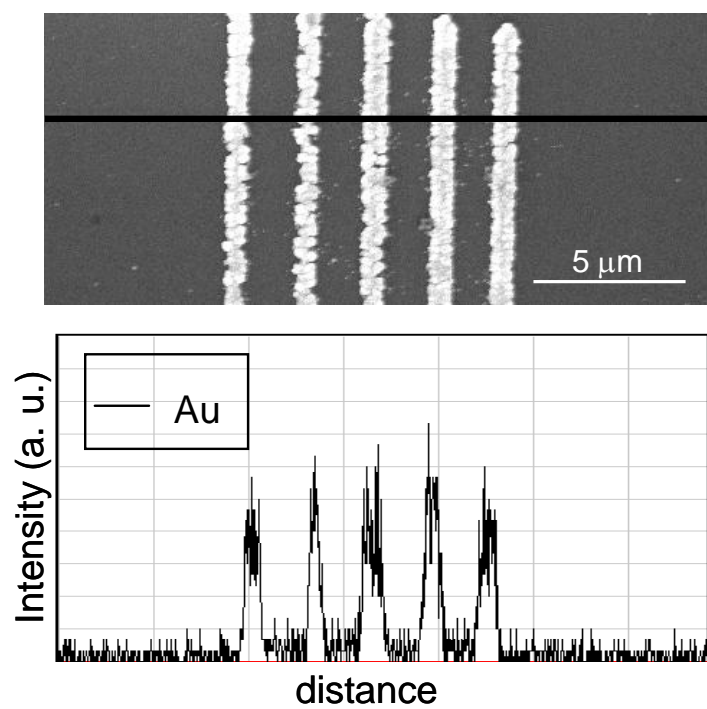| beam	irradiation current [pA]	beam width [nm]
1	10000	600
2	5000	400
3	3000	300
4	1000	100
5	500	70
6	300	50
7	100	30
8	50	20
9	10	15
10	1	8
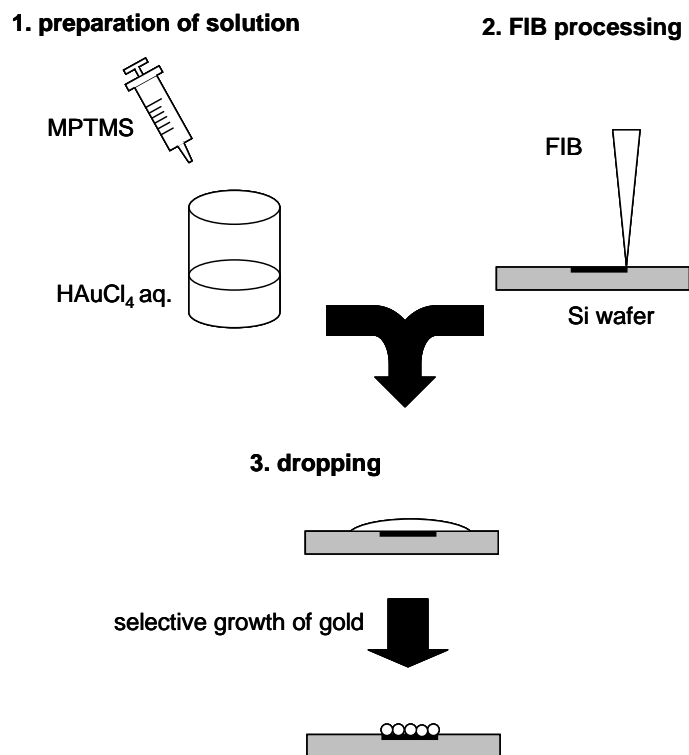
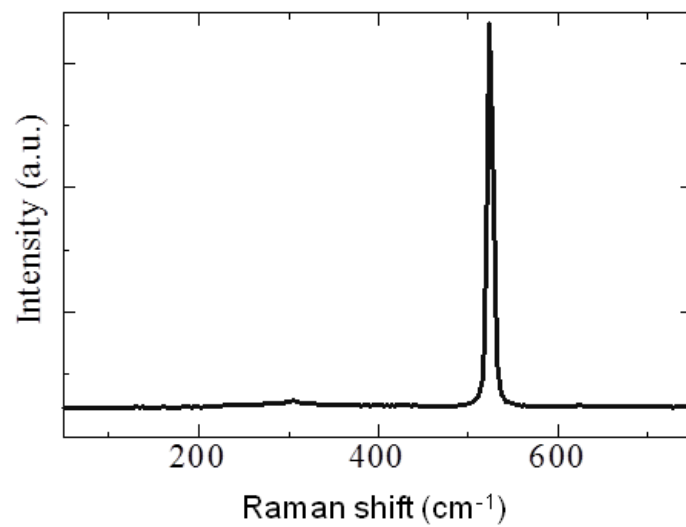**Figure 1.** Fabrication of gold patterns on Si substrate
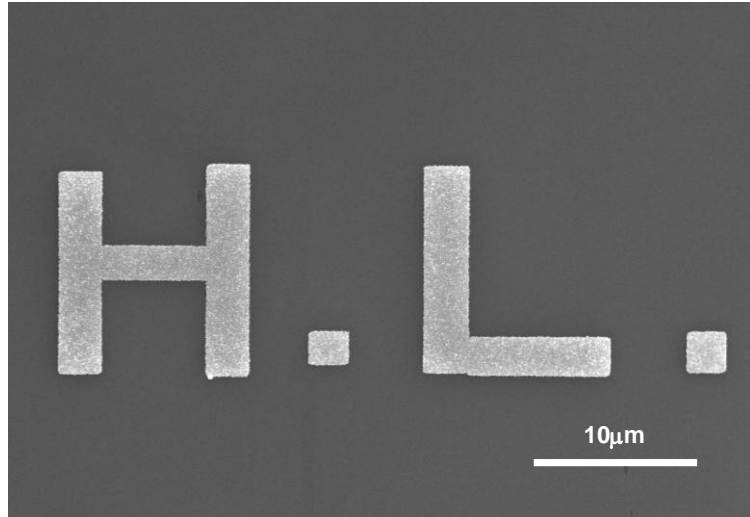
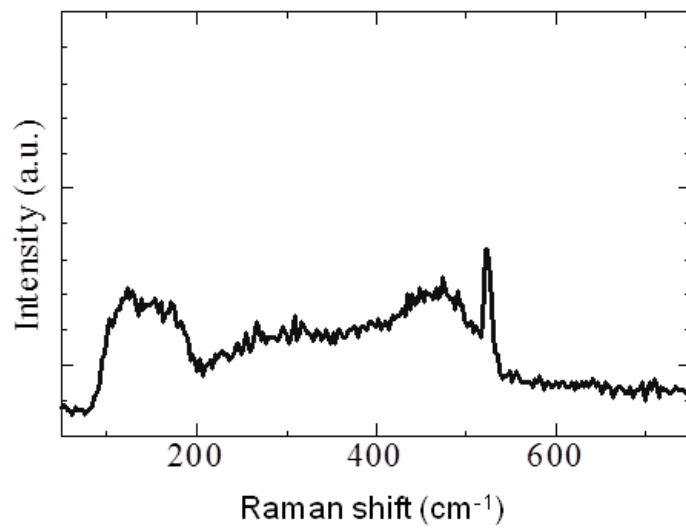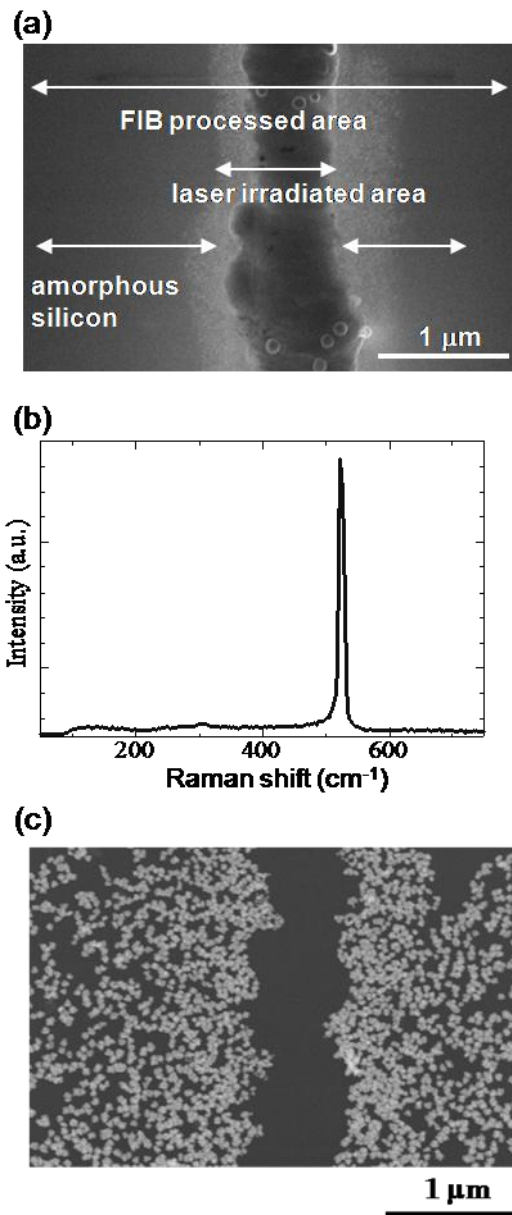**Figure 2.** FE-SEM image of a gold pattern obtained.

**Figure 3.** EDS line profile analysis of a gold structure obtained.

Figure 4. Raman spectra of unprocessed are of silicon used for gold patterning

23

Figure 5. Raman spectra of FIB-proceed are of silicon used for gold patterning.

(a)

FIB processed area

laser irradiated area

amorphous
silicon

1 μm

(b)

Intensity (a.u.)

200   400   600
Raman shift (cm⁻¹)

(c)

1 μm

Figure 6. (a) FE-SEM image of CW laser irradiated area in amorphous silicon induced by an FIB (b) Raman spectrum of CW laser irradiated area (c) FE-SEM image of same area as in (a) observed after gold precipitation.

(a)

(b)

(c)
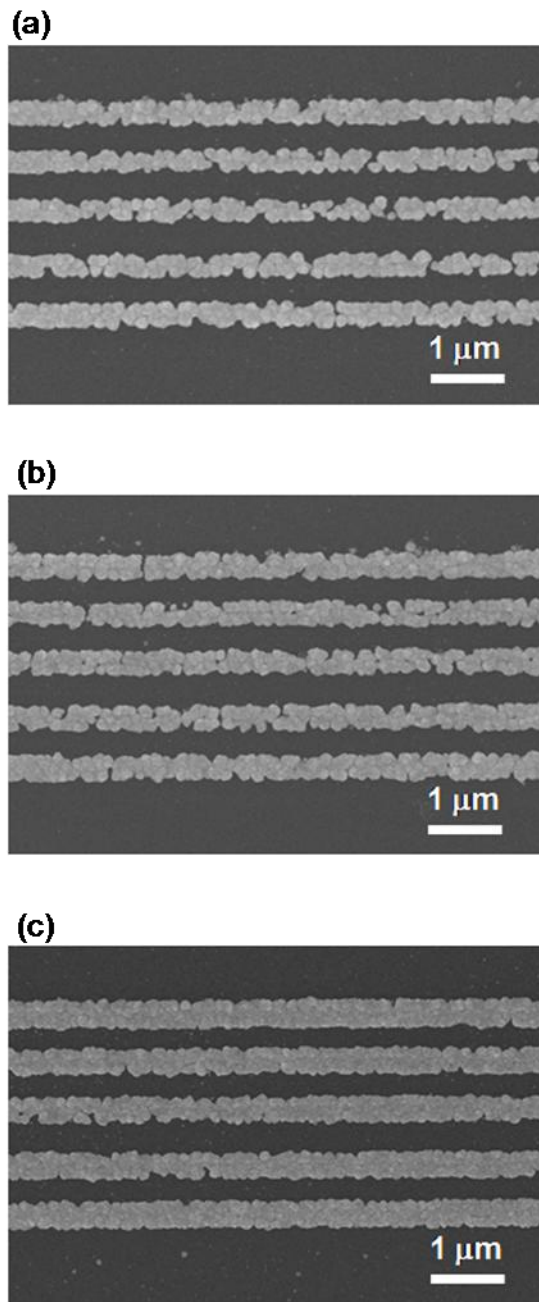
Figure 7. FE-SEM images of gold structures obtained using beam9. Estimated dosages are (a) 1.2×10^{16}, (b) 1.2×10^{17}, and (c) 3.75×10^{17} ions/cm^2.

References

[1]   M. Erhardt and R. Nuzzo, Langmuir **15** (1999), 2188

[2]   P. C. Andricacos, C. Uzoh, J. O. Dukovic, J. Horkans and H. Deligianni, IBM J. Res. Dev. **42** (1998), 567

[3]   R. Rosenberg, D. C. Edelstein, C. K. Hu and K. P. Rodbell, Annu. Rev. Mater. Sci. **30** (2000), 229

[4]   E. K. Yung, L. T. Romankiw and R. C. Alkire, J. Electrochem. Soc. **136** (1989), 206

[5]   I. Yamada, K. Takano, M. Hangyo, M. Saito and W. Watanabe, Opt. Lett. **34** (2009), 274

[6]   M. L. Brongersma, J. W. Hartman and H. A. Atwater, Phys. Rev. B **62** (2000), R16356

[7]   P. Schmuki and L. E. Erickson, Phys. Rev. Lett. **85** (2000), 2985

[8]   T. Homma, N. Kubo and T. Osaka, Electrochim. Acta **48** (2003), 3115

[9]   M. Nishi, T. Nakanishi, Y. Shimotsuma, K. Miura and K. Hirao, J. Ceram. Soc. Japan **115** (2007), 944

[10]   S. Rubanov and P. R. Munroe, J. Microsc. **214** (2004), 213

[11]   J. C. C. Fan and H. J. Zeiger, Appl. Phys. Lett. **27** (1975), 224

[12]   R. Gassilloud, C. Ballif, P. Gasser, G. Buerki and J. Michler, Phys. Status Solidi A **202** (2005), 2858

[13] L. Pelaz, L. A. Marqués and J. Barbolla, J. Appl. Phys. **96** (2004), 5947

Chapter 2

Gold patterning on silicon substrate using femtosecond laser

2.1 Introduction

Direct metal patterning on substrates (glass, semiconductor, other metal, and so on) has recently been investigated considerably [1]. A variety of applications are proposed for micro- and nano-structured metal: Interconnects for IC, Shottky diodes and wire grids for terahertz wave are common applications that come to mind immediately. MEMS (micro–electro-mechanical-system) is fabricated by integrating these components. Moreover, recent advances in nanotechnology have revealed that metal structures can act as sub-wavelength waveguides as well [2]. Most of the techniques are for electronics and optics, but we can also apply metal patterning to sensing fields. Since many groups have reported that nano-structured metal can enhance Raman signals of molecules around the surface [3], [4], metal pattering is now considered as a method for fabricating surface enhanced Raman spectroscopy (SERS)-active substrates. Since SERS-activity depends not only on the nature of metal but also on the size, shape, and particle aggregation [5], it is important to fabricate metal structure with strict control of these factors. Whatever field we aim for, developing a direct and flexible method for metal patterning is required to speed up the fabrication process and to reduce the costs.

Laser is one of the promising tools for various patterning, since it offers flexible and parallel processing in air. Several groups have reported laser-assisted methods for metal patterning: Kerner et al. employed laser desorption of a physisorbed buffer gas to pattern a grating of gold on a Ru (100) substrate under UHV condition [6]. Sun et al. showed that exposure of gold nanoparticles to UV light causes oxidation of the stabilizing molecules, leading to coagulation of the nanoparticles which consists of patterns [7]. Although these methods have great potential, it would be still important to develop other new methods since all these methods, at this stage, have both merits and demerits.

In chapter 1, I have reported a gold-patterning method using selective growth of gold nanoparticles on FIB-processed area: An aqueous solution containing aurate ion and 3-mercaptopropyltrimethoxysilane (MPTMS, used as a reductant) dropped on FIB-processed wafer produced gold nanoparticles selectively on the FIB-processed areas. The results showed that the presence of amorphous silicon phase induced by FIB-processing is important for fabricating gold nanostructures. Since amorphous silicon phase can also be induced by pulsed laser [8], there is a possibility that we could obtain the same gold structure using laser.

In this work, we attempted to achieve gold patterning on Si substrate by means of femtosecond laser. The irradiation conditions were carefully chosen according to reports from other groups so that amorphous silicon phase can be induced efficiently. To demonstrate a possibility of application of the technology to sensing, I also investigated

the SERS-activity of fabricated gold structures using rhodamin 6G (R6G) as a probe molecule.

2.2 Experimental

The process used to fabricate gold pattern is illustrated schematically in Fig. 1. Undoped Si (100) wafers were cut into 0.5 mm × 0.5 mm pieces and pre-cleaned by sonication for 5 min in ethanol. Geometric patterns were written on them with an amplified fiber laser (Ifrit, Cyber Laser) delivering 238 femtosecond pulses at 780 nm center wavelength. The repetition rate of the femtosecond laser was 1 kHz. The laser was focused on the Si (100) wafers with a microscope objective lens (NA=0.40). A drop of prepared solution was then put on the processed wafer, and the wafers were dried at 80 °C. The solution contained a mixture of 46 μl of MPTMS and 3 ml of 0.05 M aqueous solution of $HAuCl_4$ and was prepared by stirring on a hot plate set to 100 ºC for 2 h.

A Raman microspectrometer (Nanofinder30, Tokyo Instruments, Japan; wavelength=532nm, NA=0.6), a FE-SEM (JSM6700F, JEOL, Japan), and an energy dispersive X-ray spectroscope (JED-2300, JEOL, Japan) were used to investigate the processed wafers and gold structures.

For SERS measurement, R6G molecules were adsorbed by depositing a 10 μl of R6G ethanol solution (3.5×10^{-7} M) on the patterned gold structure and drying it in air. The Raman measurement was performed in back-scattering geometry. The excitation

wavelength was 532 nm and the power was kept around 5 mW.

2.3 Results and Discussion

Figure 2(a) and 2(b) show the optical microscope images of laser-processed wafers at different processing conditions: (a) 2.1 J/cm^2, 800 mm/s (b) 18.4 J/cm^2, 6500 mm/s. The fluences (2 E/$\pi\omega_0^2$) were calculated by assuming the spot size $\omega_0 = \lambda$/NA (beam waist). Figure 2(a)' and 2(b)' are optical microscope images which show the same areas as 2(a) and 2(b), respectively, but were captured after gold precipitation. Figure 3 and 4 show the Raman spectra from the processed areas of them. The contribution from amorphous silicon phase (the peak around 470 cm^{-1}) can be seen at the processed area shown in Fig. 2(a), whereas the processed area in Fig. 2(b) shows the peaks of crystalline silicon only. I have confirmed that almost the same results were obtained at 10 different points on each processed are. It is apparent that gold precipitation occurred only when amorphous silicon was induced by laser. Figure 5 shows the FE-SEM image of an obtained structure and Figure 6 shows EDS line profile analysis, which confirms that obtained structures consist of gold nanoparticles. Figure 7 shows the relation between laser fluence and gold structures obtained. This result indicates that there is an optimum range of fluence for gold nanoparticles to precipitate with high density. The highest density was achieved in the case of 16 J/cm^2. A few particles could be precipitated in the case of either below 9.5 J/cm^2 or over 32 J/cm^2. This phenomenon is consistent with the dependence of amorphization on laser fluence, which was reported by T. H. R.

Crawford et al. [9], although the amorphizable range of fluence is slightly different from mine. Probably this difference arises from the difference of laser condition. They considered that amorphization is a result of the rapid quench of silicon melts and that a dominant phase (c-Si or a-Si) at surface depends on cooling rate after laser irradiation.

These results support my mechanistical consideration. As in the case of FIB-processing, gold precipitation with high density can be achieved only when amorphous silicon phase was induced by laser. MPTMS is, in both case, considered to reduce aurate ions partially (Au(Ⅲ) → Au(0)). Partially reduced aurate ions can be completely reduced to gold nanoparticles once further energy or electrons are given from active sites of the processed area. Because severe condition is required for laser-processing to amorphize silicon compared to FIB-processing, it became more obvious in present research that amorphous silicon phase plays a crucial role in selective gold precipitation. Similar phenomenon was reported by Schmiski et al. [10]. They found that both gold and copper were deposited electrochemically only on the amorphous silicon phase induced by atomic force microscope (AFM), although it has not been revealed how amorphous phase acts on metal deposition. Since I confirmed that gold precipitation occurred on an area scratched with diamond pen (leading to surface transformation from c-Si to a-Si), it would be possible to apply our method to AFM-processing as well. Perhaps the strongest advantage of this method over other patterning methods is the flexibility of processing. We can select the most suitable tool from among three (FIB, laser and AFM) in accordance with the purpose or requirements.

The results from SERS measurement were shown in Fig. 8. The blue line is a Raman spectrum from silicon surface with R6G adsorbed, which shows no particular peaks except for a peak of c-Si. On the other hand, a Raman spectrum from the surface of a gold structure (the red line) is totally different. I can confirm several enhanced peaks in this case. These can be assigned as the peaks of R6G, not of MPTMS. These results indicate two significant points. First, the fabricated structures were SERS-active. This enhanced SERS-activity is probably due to a large number of particle junctions of gold aggregates, where strongly enhanced evanescent electromagnetic field is created. Second, the surface of fabricated gold structures is not covered with MPTMS and therefore these gold structures are suitable for SERS-active substrate.

2.4 Conclusions

I demonstrated that gold patterning on Si substrate can be performed with the assistance of femtosecond laser. Gold precipitation with high density can be achieved only when amorphous silicon phase was induced, as indicated in our previous work using an FIB. Although it is still unclear how amorphous phase acts on gold precipitation, the results imply that any processing tools can be used for this patterning method as long as it can induce amorphous silicon phase. We can select the most suitable tool from among three (FIB, laser and AFM) in accordance with the purpose or requirements. In addition, fabricated gold structures were proved to be SERS-active. Since the process is very simple and can be performed in air, I believe that this method

is a favorable candidate for fabricating SERS-active substrates.
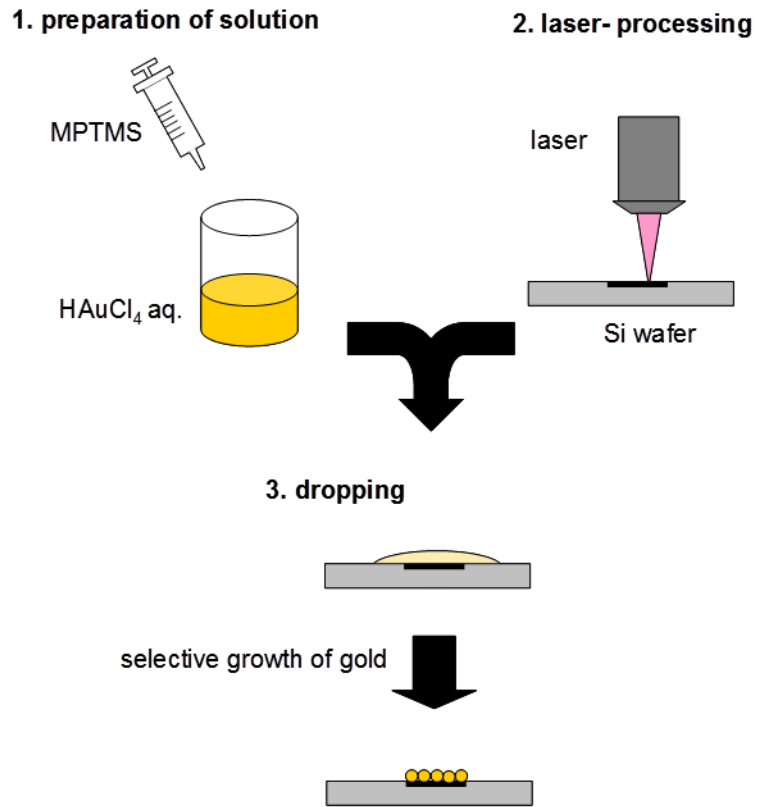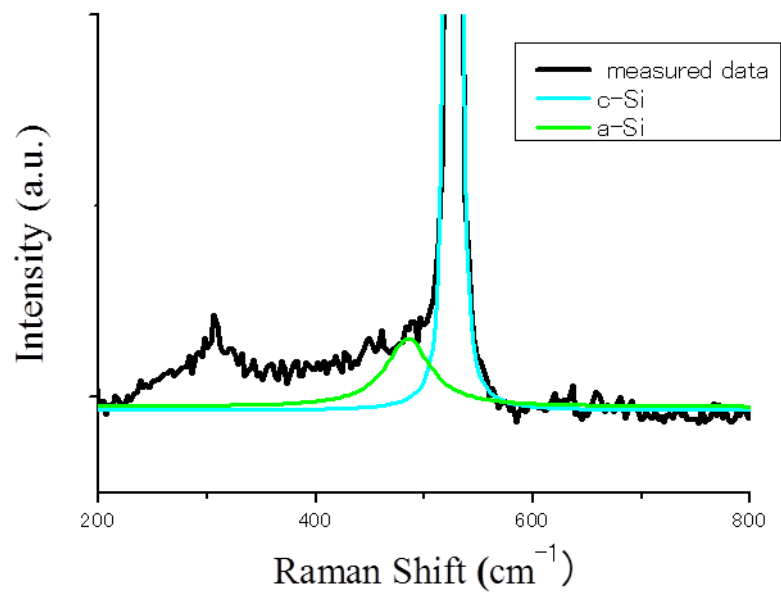
Figure 1. Fabrication process of gold pattern.
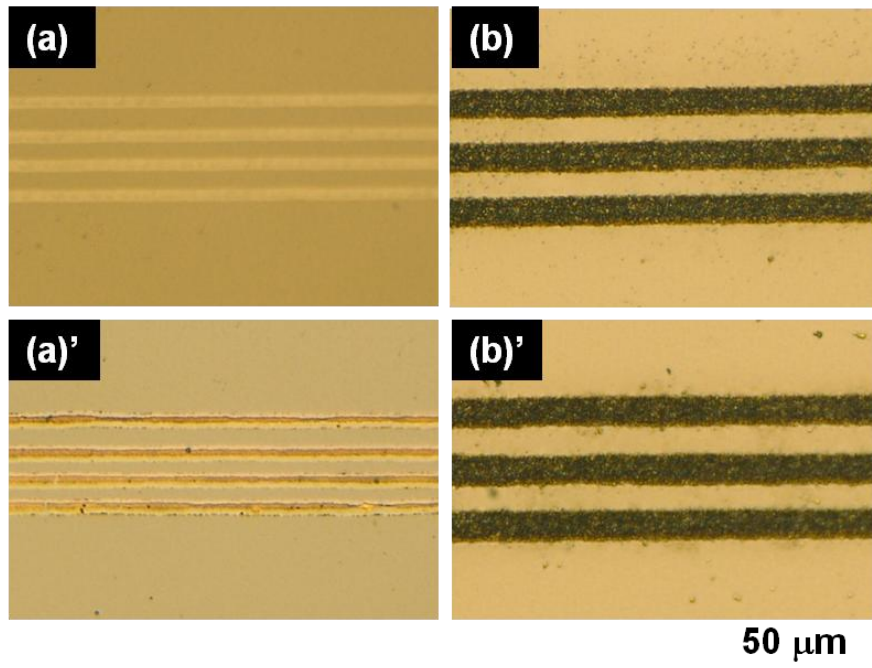
Figure 2. (a) (b): Optical-microscope images of silicon processed by femtosecond laser with different laser fluence and scan speed; (a) 2.1 J/cm^2, 800 mm/s (b) 18.4 J/cm^2 , 6500 mm/s

(a') (b'): Optical-microscope images of the same areas as (a) and (b), but captured after gold precipitation
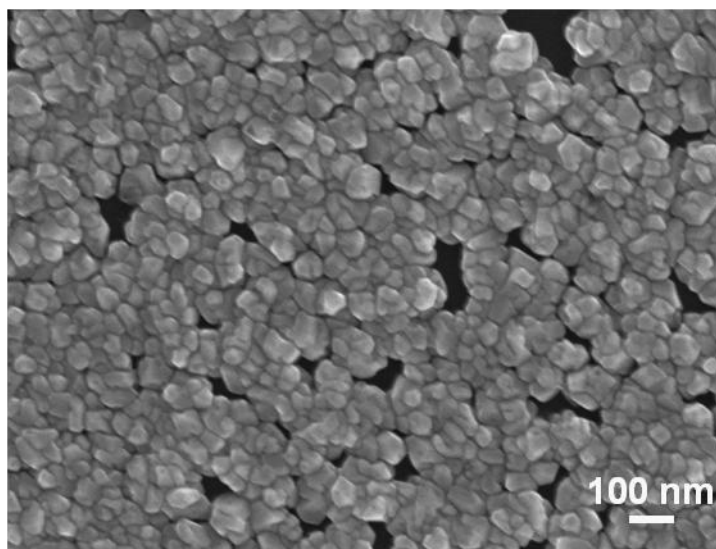
Figure 3. Raman spectra of processed areas which are shown in Figure 2(a).
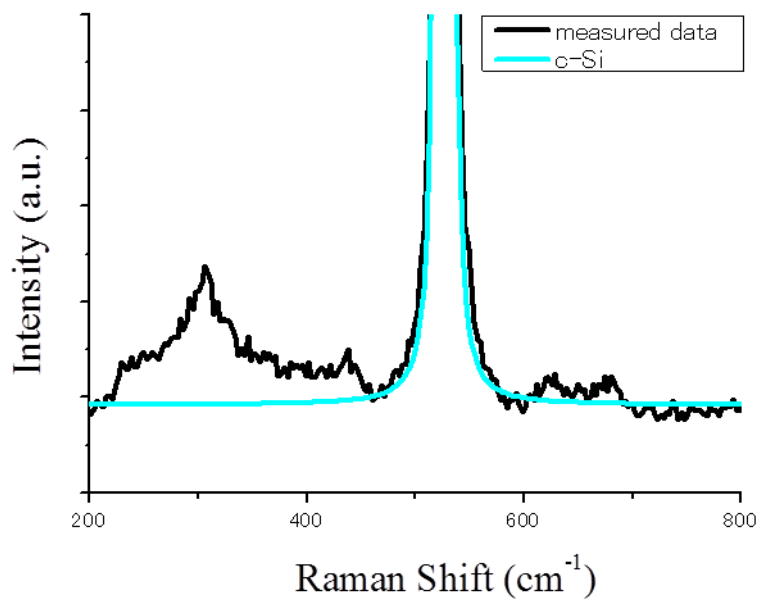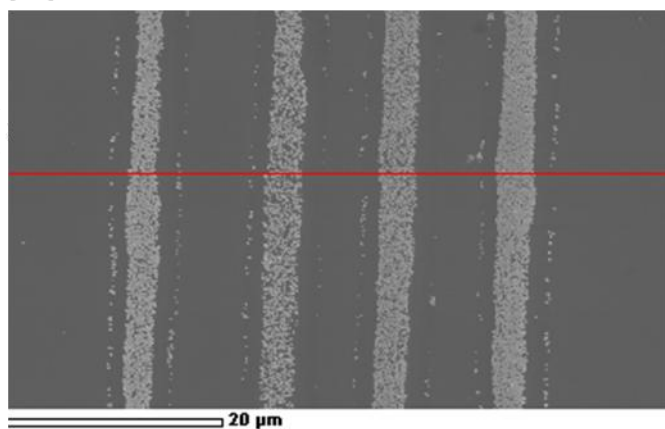
Figure 4. Raman spectra of processed areas which are shown in Figure 2(b).

Figure 5. High-resolution FE-SEM image of obtained structure.
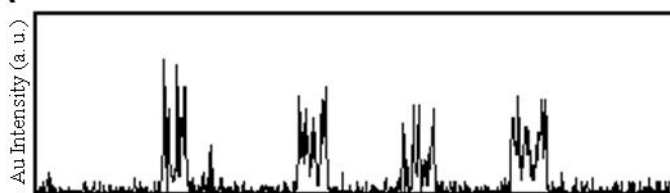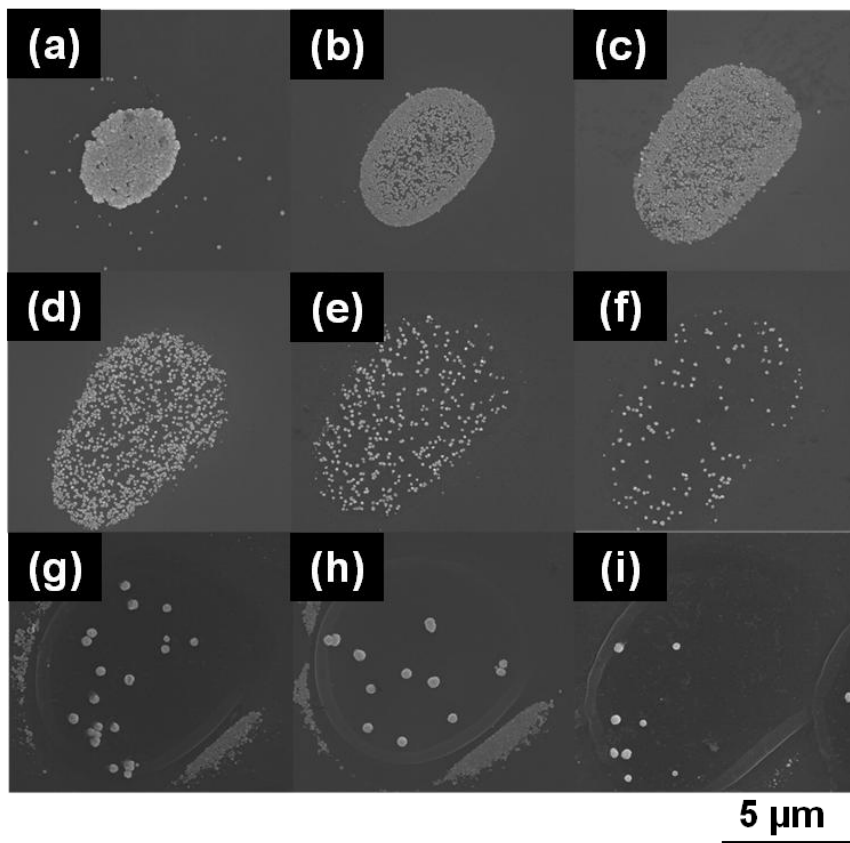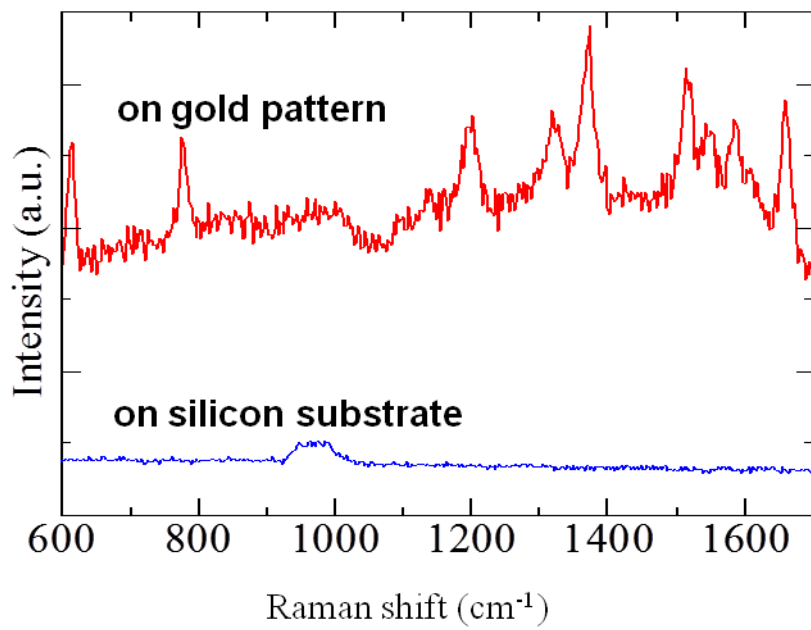
Figure 6. (a) FE-SEM image and (b) EDS line profile analysis of obtained structure.

Figure 7. FE-SEM images of obtained gold structures with different lase fluences; (a) 9.5 J/cm^2, (b) 12 J/cm^2, (c) 16 J/cm^2, (d) 22 J/cm^2, (e) 28 J/cm^2, and   (f) 32 J/cm^2.

Figure 8. Raman spectra measured on Si substrate (blue line) and on gold pattern (red line).

References and links

[1]   S. Roy, J. Phys. D: Appl. Phys. **40** (2007), R413

[2]   M. Quinten, A. Leitner, J. R. Krenn and F. R. Aussenegg, Opt. Lett. **23** (1998), 1331

[3]   M. Moskovits, Rev. Mod. Phys. **57** (1985), 783

[4]   K. Kneipp, Y. Wang, H. Kneipp, L. T. Perelman, I. Itzkan, R. R. Dasari and M. S. Field, Phys. Rev. Lett. **78** (1997), 1667

[5]   H. Xu, J. Aizpurua, M. Käll and P. Apell, Phys. Rev. E **62** (2000), 4318

[6]   G. Kerner and M. Asscher, Nano Lett. **4** (2004), 1433

[7]   S. Sun, P. Mendes, K. Critchley, S. Diegoli, M. Hanwell, S. D. Evans, G. J. Leggett, J. A. Preece and T. H. Richardson, Nano Lett. **6** (2006), 345

[8]   Y. Izawa, Y. Izawa, Y. Setsuhara and M. Hashida, Appl. Phys. Lett. **90** (2007), 044107

[9]   T. H. R. Crawford, J. Yamanaka, G. A. Botton and H. K. Haugen, J. Appl. Phys. **103** (2008), 053104

[10]   L. Santinacci, Y. Zhang and P. Schmuki, Surface Science **597** (2005), 11

Chapter 3

Facile and flexible fabrication method for SERS-active substrate using selective metal growth on silicon

3.1 Introduction

Since its first discovery by Fleischmann et al. in 1974 [1], surface enhanced Raman scattering (SERS) has been attracting more and more attention from both basic and practical viewpoints. Now that the sensitivity is proved to exceed that of fluorescence spectroscopy, along with the superior versatility, SERS is considered as one of the promising techniques for ultramicro analysis. There are two mechanisms proposed to explain the large enhancement of Raman signal; electromagnetic (EM) and chemical effects. In particular, EM effect, which arises from surface plasmon resonance of metallic nanosutructure, is of importance from practical point of view since the effect can be tuned by controlling the morphology of the structure [2]. Specifically, it has been proposed that SERS enhancement factor is mainly determined by the size of particles and the number of hot spots induced in interstitial gaps between particles [3], [4]. Thanks to recent developments, it is now possible to produce precisely controlled nanostructures and high quality SERS substrates have been demonstrated in recent years [5], [6], [7].

Many works have reported enhancement factors of more than 10^{15} and spectroscopic detection of a single molecule has been attracting considerable attentions [8], [9], [10], [11]. However, the fabrication processes involved are normally time-consuming and require expensive equipments such as electron beam lithography [12] or nanosphere lithography [13], [14], which has been hampering the practical applications. Not only that, the fact that most of the structures are fabricated on glass or used in solution means that the signal could be influenced by background peaks from these materials. Some works have reported more simple and practical method, but most of them lack precise controls over the morphology and yield structured areas much larger than required for Raman microspectroscope measurement, normally covering entire surface area of substrates, which would waste both analytes to be sensed and material used for substrates. To overcome these problems and achieve practical SERS-sensing, it is important to develop a method which enables simple and microscopic fabrication of SERS-active area on a substrate which has simple Raman spectrum such as carbon or silicon.

In previous chapters, I have reported facile fabrication method for gold pattering on Si using FIB or femtosecond laser, where FIB and femtosecond laser are used to induce defective layer on surface of Si which works as electron donor to reduce gold ions selectively on the processed areas. It can be considered as an electrodeposition process without an external voltage or current. The patterns can be fabricated at submicron scale and another advantage is that it is also possible to use other processing techniques such as a scratching machine to induce the defective layer necessary for the patterning, which

makes the method versatile and suitable for practical application. Each pattern consists

of aggregated gold nanoparticles and I found the morphology (size and aggregation) can

be changed depending on experimental conditions.

My aim in this chapter is to apply our patterning method to facile fabrication for

SERS-active substrate. I have modified the experimental method from original one in

order to obtain structures optimized for higher SERS enhancement. It was found that the

both gold and silver can be used as material to compose SERS-active nanostructure and

the morphology can be controlled by varying reaction temperature, reaction time and

concentration of the metal ion solution. I investigated the SERS-activity of each

obtained structure and confirmed that the experimental results match with simulation

results calculated using FDTD.

3.2 Experimental

Figure 1 shows a schematic representation of our fabrication method for SERS-active

substrate. Undoped Si (100) wafers (Sigma-Aldrich) were pre-cleaned by sonication for

10 min in ethanol and dried in air. Hydrogen tetrachloroaurate (III) tetrahydrate

(HAuCl$_4$ ・ 4H$_2$O) and silver(I) nitrate (AgNO$_3$) were used to prepare aqueous solutions

of metal ion with different concentrations (1.0×10^{-4}, 1.0×10^{-2}, 1.0×10^{-1} M for gold and

1.0×10^{-4}, 5.0×10^{-4}, 1.0×10^{-3} M for silver). All the chemicals were reagent grade and

used without further purification. FIB (JEM-9310, JEOL, Japan) was used to induce

defective layer on surface of Si substrate. Processing was performed at a dose of 0.5 nC

/ μm^2 and an accelerating voltage of 30 kV. In this work, the size of processing area was fixed at 5×5 μm^2. After processing, the substrates were immersed in solutions of metal ions whose temperature was maintained at 30 ˚C for gold and 10 ˚C for silver with four different reaction time (30, 60 and 120 seconds). After reaction, the substrates were gently washed with ethanol followed by drying in air. A FE-SEM (JSM6700F, JEOL, Japan) was used to observe the obtained structures.

SERS measurement was performed using a Raman microspectrometer (Nanofinder30, Tokyo Instruments, Japan; wavelength=633 nm, NA=0.6). We used thiophenol (Sigma-Aldrich) as a probe molecule to examine the SERS-activity of each obtained structure. The substrates were first cleaned by ion cleaner (JIC-410, JEOL, Japan) for 10 min to eliminate possible contamination. After cleaning, they immediately immersed in freshly prepared ethanol solution of thiophenol ($5.0×10^{-3}$ M) for 4 h, washed in ethanol for 1 min and then dried in air. I have confirmed that there is no change in SERS intensity after 4 -hour immersion, which makes it reasonable to assume that the coverage of the metal surface by thiophenol molecules is saturated in 4-hour immersion. Each spectrum was collected with the laser power of 13 mW and the collection time of 10 s. To obtain SERS enhancement factor, a spectrum was measured from undiluted thiophenol contained in square glass capillary.

3.3 Results and Discussions

The present method uses FIB to introduce defects on Si surface, which are capable of

donating electrons to gold ions. Since the energy level of defective surface can be higher than Fermi level of gold, gold ions are reduced selectively on FIB-processed areas, which have a larger number of surface defects than unprocessed area. The overall redox reaction can be written;

$$AuCl_4^- + 3e^- \rightarrow Au^0 + 4Cl^-$$

$$\equiv Si \cdot + H_2O \rightarrow \equiv Si - OH + H^+ + e^- \qquad (1)$$
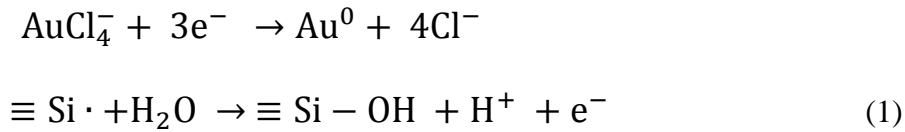
Here I assume that the subsequent nucleation and growth steps can be described in similar manner used in the field of electroplating [15].

Figure 2 shows the gold nanostructures obtained under each different condition. Here all the structures can be viewed as 2-dimensionally aggregated gold nanoparticles. With this viewpoint, the size of particle and the degree of aggregation increased as increasing the concentration of gold ion. Similar trend was found as increasing the reaction time. Generally, the morphology is determined by competitive two steps; nucleation and growth. When the concentration is low, the rate of nucleation as well as the rate of following growth are slow because of the small driving force for both steps described as Nernst equation;

$$E = E^0 + \frac{RT}{zF} \ln \frac{a_{ox}}{a_{Red}} \qquad (2)$$

leading to less aggregation and smaller particles. It can be seen the growth becomes dominant as reaction time increases. On the other hand, as increasing the concentration of gold ions, both steps are promoted, which leads to the highly aggregated structures. It should be noted that when a solution with higher concentration and longer reaction

time was employed, gold covered the whole surface of processed area and second or third layer of the gold appeared. The reason why the solution with highest concentration yields less amount of gold with poor aggregation can be explained by the Equation (1): Since the silicon oxidation is associated with release of proton, the equilibrium is shifted toward left when a solution with lower PH is used, which results in the less donation of electron in the system. As can be seen below, it is not the case when silver nitrate (AgNO$_3$) is used.

Figure 3 shows the Ag nanostructures obtained. Compared to gold particle, silver particle tended to grow larger with less aggregation, which indicates that the nucleation rate was low. The average particle sizes measured from SEM images were in a range from 15 to 78 nm for gold particles and from 13 to 250 nm for silver particles. I speculate that these differences between two metals arise from the differences of physical factors associated with nucleation and growth, such as reduction potential, surface free energy and rate of ion diffusion.

Figure 4 shows the Raman spectra collected on each gold nanostructure. The comparison of the spectra reveals that each structure shows different SERS effects and the maximum enhancement was obtained from structure with largest particles. The peaks at 1001 (C-C symmetric breathing mode), 1024 (C-C asymmetric breathing mode), 1077 (C–C symmetric breathing mode and C-S stretching mode), 1575 (C-C stretching mode in the ring) cm^{-1} can be assigned to that of thiophenol. Two prominent differences between SERS and normal Raman spectrum of thiophenol (data not shown)

was found: The intensity of the C-C stretch increased relative to the symmetric breathing mode and the C-S mode at 1077 cm^{-1} was shifted and strongly enhanced, which are typical for SERS spectra of thiophenol [16]. As can be seen in Fig. 5, the silver structures show similar trend of size-dependence although the maximum enhancement was obtained from the sample with second largest particles, not from one with the largest particles. The data also shows that the enhancement is larger for silver structures than for gold structures.

FDTD calculations were performed on a commercial FDTD package to evaluate the size- and material- dependence of local electromagnetic fields at the excitation wavelength of 633 nm in the same manner used by P. P. Fang et al. [17] Since the particle density in our substrate is sufficiently high, I assumed the enhancement effect for a measured area is determined by a field enhancement originated from interparticle plasmon coupling at a junction between two particles, which is known to be two order of magnitude larger than the maximum electric field enhancements for a single nanoparticle [3], [4], [18], [19]. The size of the particle was varied in a range from 10 to 150 nm with a fixed interparticle distance of 2 nm. Polarization of incident field was set to be parallel to the dimer axis. Figure 6 shows the size-dependent field enhancement at junctions of gold and silver dimers. The calculated results show that there is a little difference in field enhancements between gold and silver. Both metals reach the maximum field enhancement where the size of particle is around 120 nm. Since Raman enhancement is considered to depend on the forth power of the induced electric field in

51

this case, I also calculated $|E|^4$ as a function of particle size and plot the calculated results with the experimental values (Fig. 7). According to the calculated results, the main factor giving rise to a difference between gold and silver structures is thought to be the size of the particles. The difference in shape may be another factor since SERS enhancement becomes larger if the particle has sharp protrusion points [2]. As can be seen in Fig. 2 and 3, my silver samples have more protrusions than gold samples. The results also explain why the maximum SERS intensity among silver samples is obtained from the sample with second largest particles. Since electric field enhancement of a metal nanoparticle depends on the competing effects of radiation damping and dynamic depolarization of surface plasmon [20], there exists an optimal size for SERS enhancement and it is about 120 nm, which corresponds to the second largest size.

For evaluation of SERS-activity, I calculated the enhancement factors given by;

$$EF = \frac{I_{SERS}/N_{SERS}}{I_{bulk}/N_{bulk}} \qquad (3)$$

where I_{bulk} and I_{SERS} are the Raman intensities taken from liquid thiophenol and a SERS substrate, respectively. We used the peak intensities at 1077 cm^{-1} since it can be considered as a good indicator for SERS effect. N_{bulk} and N_{SERS} represent the number of molecules probed by the laser spot: For N_{bulk}, I assumed Raman signals were collected from thiophenol molecules which occupy a focused volume V of laser beam generally expressed as;

$$V = \pi w_0^2 \times d \qquad (4)$$

52

where w_0 is a beam waist and d is depth of focus, which is given by;

$$d = \frac{\lambda}{NA^2} \tag{5}$$

where λ is a wavelength of laser (633 nm in this work) and NA is a numerical aperture of the object lens. Using the calculated V and the density of liquid thiophenol, we can estimate N_{bulk}. Since the SERS peak intensity was saturated after immersion for 4 h, it should be reasonable to assume full coverage of thiophenol over the metal surface. Therefore, I used a value of 0.53 nmol cm^{-2} for N_{SERS} in my experiment, which is one of the reasonable values for surface density of thiophenol reported elsewhere [21]. Using these values, the obtained maximum enhancement factors are 10^5 for silver and 10^4 for gold.

3.4 Conclusions

I applied my metal patterning method to facile fabrication for SERS-active substrate. Both gold and silver structures showed reasonable SERS enhancement and we found there is an optimal size of particles determined by dielectric constant of the metal and the wavelength used for excitation. Since the size and the degree of the metal structures can be easily controlled by varying experimental condition such as reaction temperature, reaction time and concentration of the metal ion solution, we can optimize the structure depending on which laser is available and which metal is more suitable for analytes to be sensed. We believe the simplicity and flexibility of our method will be a advantage over other existing methods for fabrication of SERS-active substrate and the method
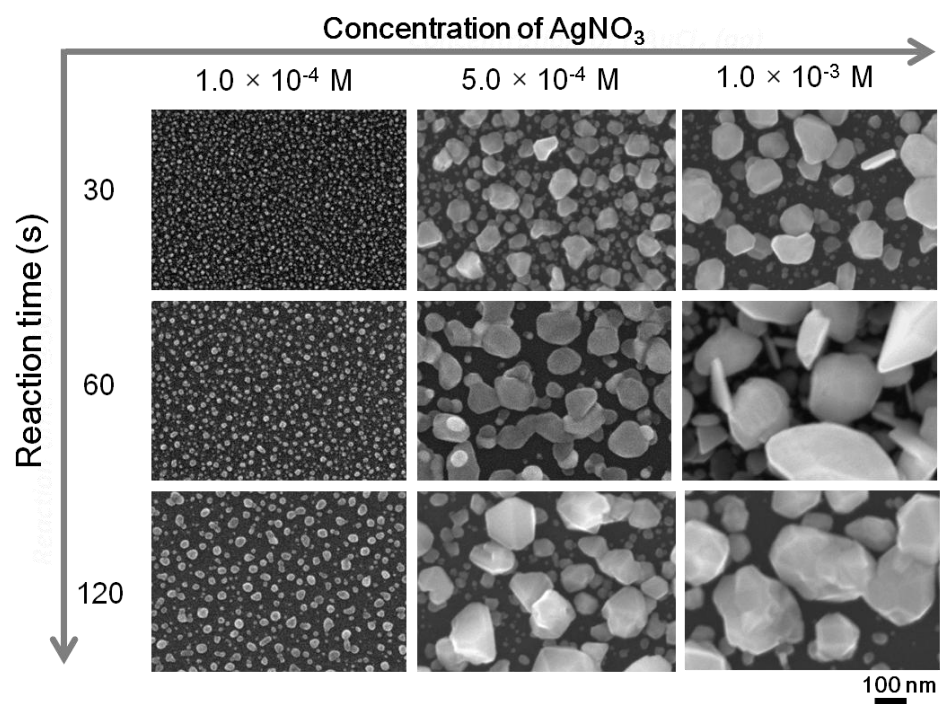
will contribute to future development of SERS sensing.
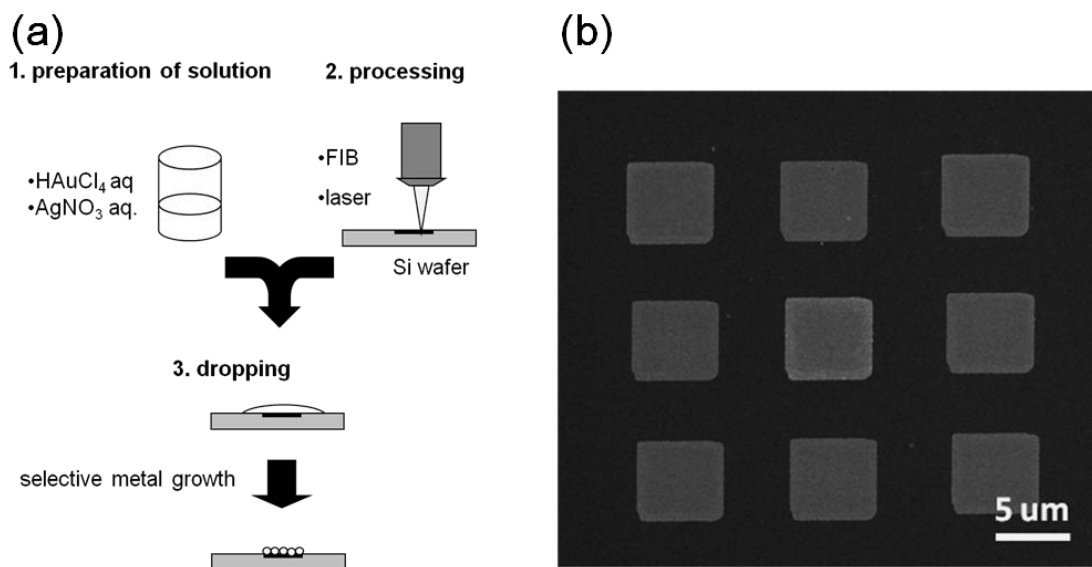
Figure 1. (a) Schematic representation of the fabrication method used in this work to prepare gold and silver structures on silicon substrate. **(b)** FE-SEM image of a obtained gold structure.
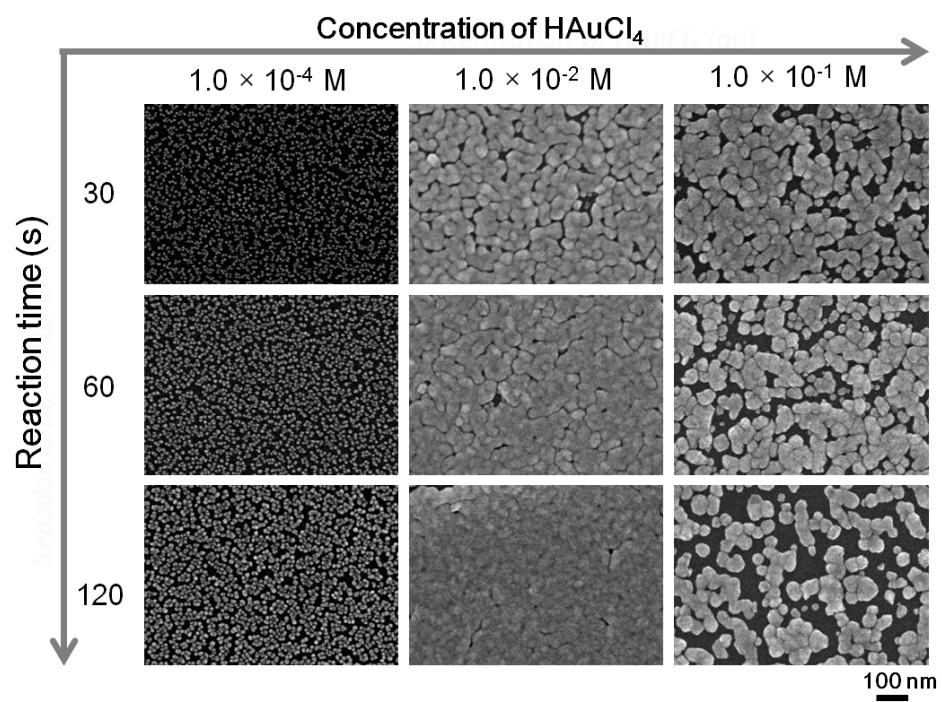
Figure 2. FE-SEM images of obtained gold structures with different reaction time and concentration of gold ion.
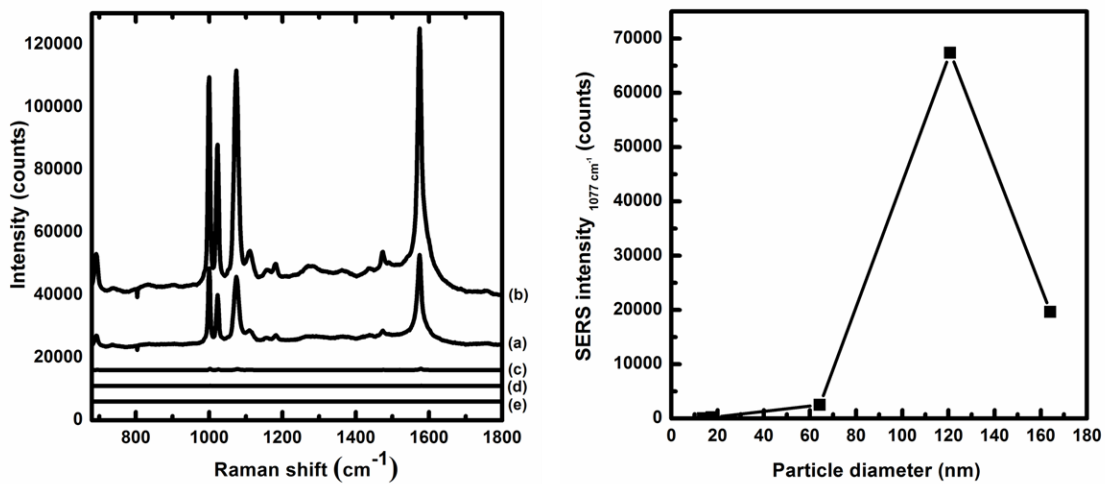
Figure 3. FE-SEM images of obtained silver structures with different reaction time and concentration of silver ions.
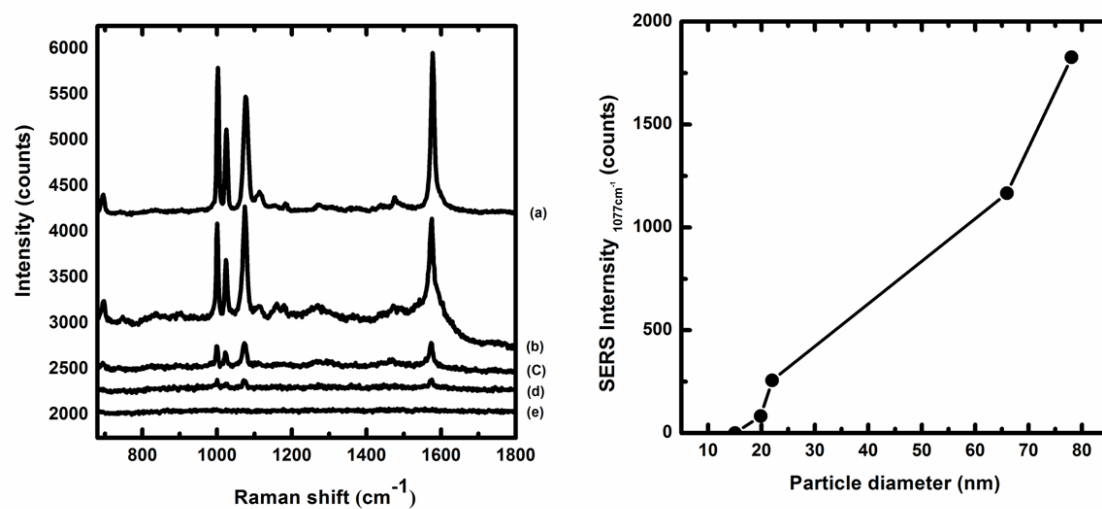
Figure 4. SER spectra (left) collected from fabricated gold structures whose average particle size are (a) 78, (b) 66, (c) 22, (d) 19 and (e) 15 nm. The right figures are plots of SERS intensity at 1077 cm^{-1} as the particle size.

Figure 5. SER spectra (left) collected from fabricated silver structures whose average particle size are (a) 164, (b) 121, (c) 64, (d) 17, (e) 13 nm. The right figures are plots of SERS intensity at 1077 cm^{-1} as the particle size.
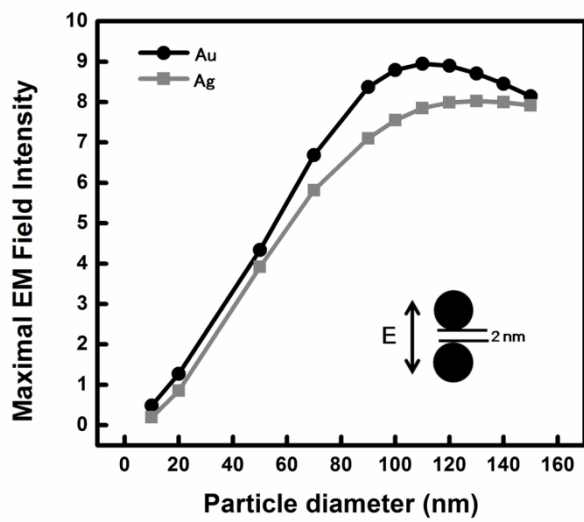
Figure 6. Maximal electromagnetic field intensity calculated using FDTD.
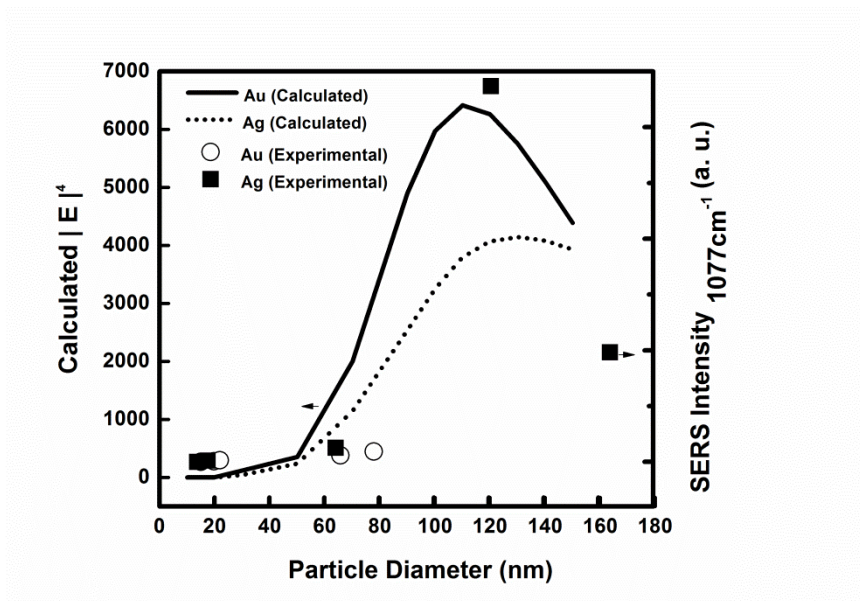
Figure 7. Comparison between calculated $|E|^4$ values and experimentally-obtained SERS intensities at 1077 cm^{-1}.

References

[1]   M. Fleischmann, P. J. Hendra, A.J. McQuillan, Chem. Phys. Lett. 26 (1974), p. 163

[2]   Hongxing Xu et al. Phys. Rev. E **62** (2000), 4318

[3]   J. Jiang, K. Bosnick, M. Maillard, and L. Brus, J. Phys. Chem. B **107** (2003), 9964

[4]   P. K. Jain and M. A. El-Sayed, Chem. Phys. Lett. **487** (2010), 153

[5]   X. M. Lin, Y. Cui, Y. H. Xu, B. Ren and Z. Q. Tian, Anal Bioanal Chem. **394** (2009), 1729

[6]   B. Yan, A. Thubagere, W. R. Premasiri, L. D. Ziegler L. D. Negro and B. M. Reinhard, ACS NANO **3** (2009), 1190

[7]   A. Gopinath, S. V. Boriskina, W. R. Premasiri, L. Ziegler, B. M. Reinhard and L. D. Negro, Nano Lett. **9** (2009), 11

[8]   K. Kneipp, Y. Wang, H. Kneipp, L. T. Perelman, I. Itzkan, R. R. Dasari and M. S. Feld, Phys. Rev. Lett. **78** (1997), 1667

[9]   K. A. Bosnick, J. Jiang and L. E. Brus, J. Phys. Chem. B **33** (2002), 106

[10]   X. M. Qian and S. M. Nie, Chem. Soc. Rev. **37** (2008), 912

[11]   D. K. Lim, K. S. Jeon, H. M. Kim, J. M. Nam and Y. D. Suh, Nature Materials **9** (2010), 60

[12]   E. C. Le Rua, P. G. Etchegoina, J. Grandb, N. Félidjb, J. Aubardb, G. Lévib, A. Hohenauc and J. R. Krennc, Current Applied Physics **8** (2008), 467

[13] L. Baia, M. Baia, J. Popp and S. Astilean, J. Phys. Chem. B **110** (2006), 23982

[14] B. G. Prevo and O. D. Velev, Langmuir **20** (2004), 2099

[15] E. Budevski, G. Staikov and W. J. Lorenz, Electrochimica Acta **45** (2000), 2559

[16] M. K. Kinnan and G. Chumanov J. Phys. Chem. C **111** (2007), 49

[17] P. P. Fang, J. F. Li, Z. L. Yang, L. M. Li, B. Ren and Z. Q. Tian, J. Raman Spectrosc. **39** (2008), 1679

[18] M. Futamata, Y. Maruyama and M. Ishikawa, J. Phys. Chem. B **107** (2003), 7607

[19] J. M. McMahon, A. I. Henry, K. L. Wustholz, M. J. Natan, R. G. Freeman, R. P. V. Duyne and G. C. Schatz, Anal Bioanal Chem. **394** (2009), 1819

[20] M. Meier et al. Opt. Lett. **8** (1983), 11

[21] L. J. Wan, M. Terashima, H. Noda and M. Osawa, J. Phys. Chem. B **104** (2000), 3563

Chapter 4

Functionalization of SU-8 surface for fluorescent or SERS sensing

4.1 Immobilization of materials on SU-8 surface using sol-gel technique

4.1.1 Introduction

SU-8 is an epoxy-based negative photoresist and originally developed for the microelectronics industry to provide a high-resolution mask for fabrication of semiconductor devices. Since it enables the production of high-aspect-ratio structures, SU-8 is now used in a wide range of fields for the fabrication of 3D structures, especially in the fabrication of microfluidics and microelectro-mechanical systems (MEMS) [1], [2], [3], [4]. It is also suitable material to fabricate 3D structures with sub-micron features by using two-photon polymerization technique [5], [6], [7], which has currently been attracting much attention in the field of optical trapping [8]. Despite the excellent mechanical properties, thermal and chemical stability, and biocompatibility of the polymerized SU-8 structures, it remains difficult to realize practical microsystems using SU-8 as building blocks because there are still only a few techniques available for

functionalization of the surface. It has been required to develop simple and effective method to functionalize the surface of SU-8 with various materials, especially with environmentally-responsive materials for sensing.

Conventionally, most of optical sensing techniques are based on organic molecules which show qualitative change in absorption or emission upon specific environmental changes. Among them, oxygen, PH, and calcium indicators are widely used. Recently, Surface Enhanced Raman Scattering (SERS) has been proved to be an effective and versatile technique to detect small amount of molecules in samples [9], [10], [11]. Raman signal of one molecule is normally too weak to detect, but SERS utilizes metal nanostructures to enhance electromagnetic field in close proximity to surface so that the signal can be sufficiently enhanced for detection. SERS substrates are typically fabricated by functionalizing glass or silicon substrates with gold or silver nanoparticles [12], [13], [14]. It should also be possible to make the surface of SU-8 SERS-active by developing a method to functionalize SU-8 with metal nanoparticles.

Several groups have been working on functionalization of SU-8 with bio-molecules or inorganic particles [15], [16], [17], [18]. Most of them are based on chemical adsorption of material on bare or modified surface of SU-8. For homogeneous and strong adsorption, it is preferable to form covalent bonds between the surface and functional materials. However, because the each method is designed only for a specific chemical reaction, it is required to redesign the method when the material to functionalize is changed. To avoid this, porous materials can be used as a host matrix to entrap probe molecule or

particles without direct bond formation with the surface. One of the most-used porous material is a silica-based xerogel, which can be obtained by sol-gel method. The process to form the gel film is simple and can proceed under mild condition. Various functional materials can be added into the sol and they get entrapped inside gels during the gel-forming process [19], [20]. The highly porous nature of sol-gel materials makes them excellent hosts for sensing materials, especially for bio-sensing, since the species to be sensed can easily diffuse towards the sensing center while the matrix improves biocompatibility by protecting the biological environment from any toxic effects of the sensing materials. Furthermore, it is potentially possible to functionalize the surface of substrate with any dyes or particles by entrapping them inside gel as long as the gel stably adheres on the surface via covalent bond.

In this work, I functionalized the surfaces of photopolymerized SU-8 by coating them with silica-based xerogel prepared with a fluorescent calcium indicator or gold nanoparticle. I first investigated the adhesion strength of coating, as well as the chemical states of the SU-8 surface and gel film. Because the hydrophobic and inert surface of SU-8 is not expected to allow desired wetting of the hydrophilic silica-sol, I chose a sol composition which contains a cationic surfactant, cetyltrimethylammonium bromide (CTAB), to enable smooth coating on SU-8. It works not only as a pore-forming agent, but also as a surfactant to change the wetting property of the sol on hydrophobic structures. The response test was conducted using fluorescent spectroscope for the film with calcium indicator and Raman spectroscope for the film with gold

nanoparticles in order to demonstrate the effectiveness of the method.

4.1.2 Experimental

1. SU-8 film preparation

SU-8 films used in this work were prepared following a typical procedure: Unexposed SU-8 3035 (NIPPON KAYAKU) was first spin-coated on a cover glass substrate and pre-baked at 95 ˚C for 1 h. The substrate was then exposed to UV lamp (365 nm) with the exposure energy of 3×10^2 mJ/cm^2. After the exposure, the substrate was post-baked at 95 ˚C for 15 min, followed by developing for 15 min in a SU-8 developer (NIPPON KAYAKU) and rinsing with isopropanol.

2. Silica sol preparation

Preparation of sol-gel solution for coating was performed according to the work reported in literature [21]. A prehydrolysed solution was prepared by heating an ethanolic solution containing tetramethoxysilane (TMOS), water and hydrochloric acid in the following molar ratio: 1 TMOS: 3 EtOH: 5×10^{-5} HCl: 1 H$_2$O at 100 ˚C for 1 h. Then, cetyltrimethylammonium bromide (CTAB) was dissolved in ethanol and added to the prehydrolysed solution together with an additional amount of water and HCl. The final molar ratio was 1 TMOS: 20 EtOH: 0.004 HCL: 5 H$_2$O: 0.10 CTAB. The final solution was then stirred for four days at room temperature. For the fluorescent response test, a calcium indicator (Fluo-5N, invitrogen) was added to the sol while stirring in an amount

to give 0.13 mM of the dye concentration in final solution. For the SERS response test, gold nanoparticles were prepared according to a work reported by Wu et al. [22], which gives a method to synthesize star-shaped gold nanoparticles. The prepared particles were washed in ethanol and then added to the sol while stirring.

3. Coating and heat treatment

The prepared sol was spin-coated on the post-baked SU-8 films at 500 rpm for 5 s and 2000 rpm for 20 s. The films were then baked on a hot plate at 100 ˚C for 1 h and 150 ˚C for 1 h. For comparison, the films without heat treatment were also prepared by drying them at room temperature for 24 h.

4. Analysis

The adhesion strength of the coating was evaluated by a method called cross-cut tape test: 6×6 slits were made on the coating film at 1 mm intervals with a blade. An adhesive tape (with adhesive strength of 10±1 N per 25 mm width) with a length of approximately 50 mm was then applied to the areas and pulled off rapidly to see whether the adhesion is strong enough. To make it easier to recognize, the coating film was prepared with fluorescent dye (Rhodamine 123) for this test. Chemical states of the SU-8 surface were investigated by XPS (X-ray pfhotoelectron spectrrosxope). The spectra were acquired using an ULVAC-PHI 5500MT system at room temperature with Mg Kα radiation (15 kV, 400 W). The electron take-off angle was set at 45 deg. Binding energies were referenced to C 1s level of residual graphitic carbon. Raman

microspectrometer (wavelength=633 nm) was also used to analyze the SU-8 films. Fourier transform infrared (FTIR) spectra of the SU-8 film and silica gel film formed on the SU-8 were characterized using an IR spectrophotometer with the diamond attenuated total reflection (ATR) prism.

5. Response test

The response of the gel film with fluorescent calcium indicator was evaluated using a spectrofluorometer (Fluoromax-P, Jobin Yvon Horiba) with excitation at 490 nm. These fluorescence spectra were measured by first immersing the structures or the film into solutions with various concentrations of calcium ions for 10 min and then drying them in air for a few minutes. The response of the gel film with gold nanoparticle was evaluated using Raman microspectrometer (wavelength=633 nm). We used thiophenol (Sigma-Aldrich) as a probe molecule to examine the SERS-activity of the entrapped gold nanoparticles. The film was immersed in freshly prepared ethanol solution of thiophenol (5.0×10^{-3} M) for 4 h, washed in ethanol for 1 min and then dried in air before use.

4.1.3 Results and Discussions

In this work, I used CTAB not only as a pore-forming agent, but also as a surfactant to improve wetting property of the sol on the SU-8 surface. Additionally, I also chose ethanol as solvent because it has good wetting property on polymer surface. Figure 1

shows the differences arising from sol composition. The reference sol does not contain CTAB and consists of TMOS, water, HCl and methanol. A clear difference of the wetting behavior of the sol on SU-8 was observed. In fact, it was impossible to coat the SU-8 using the reference sol because of the poor wetting.

Figure 2 shows the optical images of the areas which were taken before and after tape removal. While the most part of the coating on grid square was detached from the sample without heat treatment (Fig. 2(c)), none was detached from the sample with heat treatment at 100 ˚C for 1h and 150 ˚C for 1 h (Fig. 2(d)). The substantial improvement in adhesion strength may indicate the formation of covalent bond between the gel film and SU-8 due to heat treatment. I used XPS, Raman spectroscopy and FTIR to obtain further information about the chemical state of the materials involved. Figure 3 is the C1s XPS spectra measured on the surface of SU-8 with different heat treatment condition. Figure 3(a) was from the sample without heat treatment, 3(b) was from the sample baked at 100 ˚C for 2 h and 3(c) was from the sample baked at 100 ˚C for 2 h and 150 ˚C for 2 h. From the fitting results, it can be seen that a large peak at 286.3 eV decreased in peak area as the heat treatment progressed. Instead, the new peak at 285.9 eV appeared and became dominant. The two peaks at 286.3 eV and 285.9 eV can be assigned to the peaks from epoxy ring and ethers respectively [18], [23], which indicates that there are considerable amounts of unreacted epoxy rings before heating and they were opened by the heat treatment. Raman spectra in Fig. 4 also show that the intensities of the peaks from epoxy ring at 1252 and 920 cm^{-1} decreased relative to the

intensity of the peak from benzene ring at 1610 cm^{-1} as the heat treatment progressed [24],

[25]. The similar trend was confirmed in the FTIR spectra (Fig. 5) measured on the

surface of SU-8, where the peak intensity at 910 cm^{-1} (epoxide deformation peak [26], [27])

also decreased. The evidences to support that epoxy rings are still present even after

post baking have also reported by other groups [15], [18], [28]. I measured the FTIR spectra

on the SU-8 coated with silica gel (Fig. 6). Although the direct evidences of the

covalent bond formation (i.e., Si-O-C bond formation) are difficult to obtain, it can be

seen that the peak from Si-OH decreased as baked. On the other hand, the peaks from

Si-O-Si increased, which indicates strengthening of silica network in gel films. It is

reasonable to consider that the Si-O-C bond between silica gel and the surface of SU-8

was also formed during the heat treatment: After spin-coating, there are enough

amounts of unreacted Si-OH in the gel as well as epoxy rings on the surface of SU-8,

and an enough amount of heat for Si-O-C bond formation was given to the reaction

system. Several works have reported Si-O-C bond formation during sol-gel reaction of

silanoxy compounds with polymer containing epoxy groups in this temperature range

[29], [30]. Therefore, I conclude that the improvement in adhesion strength by heat

treatment is mainly associated with the Si-O-C bond formation at the interface between

the gel film and SU-8.

Since the adhesion strength of coating was found to be strong enough, I tried to coat

only local area of microstructure fabricated by two-photon polymerization. Figure 7(a)

is the schematic representation of the procedure. For recognition, Rhodamine 123 was added to the sol during preparation. Figure 7(b), (c) and (d) are optical microscope images of the fabricated structure. Figure 7(b) was taken under white illumination while 7(c) was taken with 532 nm CW laser. Figure 7(d) was also taken under green laser illumination, but observed with high-pass filter which rejects radiation below 540 nm. The results indicate that the coating method for functionalization can be applied to local coating of microstructures, which expands possibilities for fabrication of microsystems.

Figure 8 shows the fluorescence emission spectra of the gel film coated on a cover glass. It can be seen that the entrapped calcium indicator in gel matrix exhibits an emission band around 530 nm whose intensity depends on the concentration of calcium ion. It is clear that the entrapped dyes remain sensitive in the gel matrix. I also confirmed that the response was reversible and reproducible even after several measurement cycles. Although there was also the leaching of dye molecules out of the matrix to some extent, we think this is not of much concern for short time or disposable use of the sensors.

Figure 9 shows the optical and SEM images of the film with gold nanoparticles. I can see that the size of individual particle is around 80 nm and the particles form aggregates whose size is are around 500 nm. These aggregates were uniformly distributed over the obtained film and the film looked transparent to the naked eye. After immersing these films in dilute ethanol solution of thiophenol, we measured Raman spectra on the films

(Fig. 10). The spectrum in black line was measured on the film with gold nanoparticles and the gray was from the film without gold nanoparticles. Strong peaks from thiophenol were detected on the film with gold nanoparticles, while none of these peaks were detected on the film without gold nanoparticles. From these results, it is clear that the entrapped gold nanoparticles retain its responsiveness as SERS material in the gel similarly to the case of calcium indicator.

4.1.4 Conclusion

I have functionalized surfaces of photopolymerized SU-8 by coating them with silica-based xerogel prepared with a fluorescent dye or gold nanoparticle. In both cases, the materials entrapped inside silica gel retain the responsiveness. The heat treatment after spin coating was found effective in improving adhesion and hardness of the obtained films. From XPS, Raman spectroscopy, and FTIR measurement, the substantial improvement can be explained by covalent bond formation between the SU-8 surface and gel film. The sol-gel matrix contained only one dye in this work, but multiple dyes can also be combined in a single matrix, so that a reference standard can be used to minimize possible errors. Additionally, we can potentially entrap any dye inside the matrix. Other nanoparticles, quantum dots and even enzymes can also be entrapped. Since this simple method enables us to functionalize various functional

materials on surfaces of SU-8, we believe that it will be a promising way to fabricate

MEMS sensors or micro-TAS (total analysis system) devices based on SU-8.
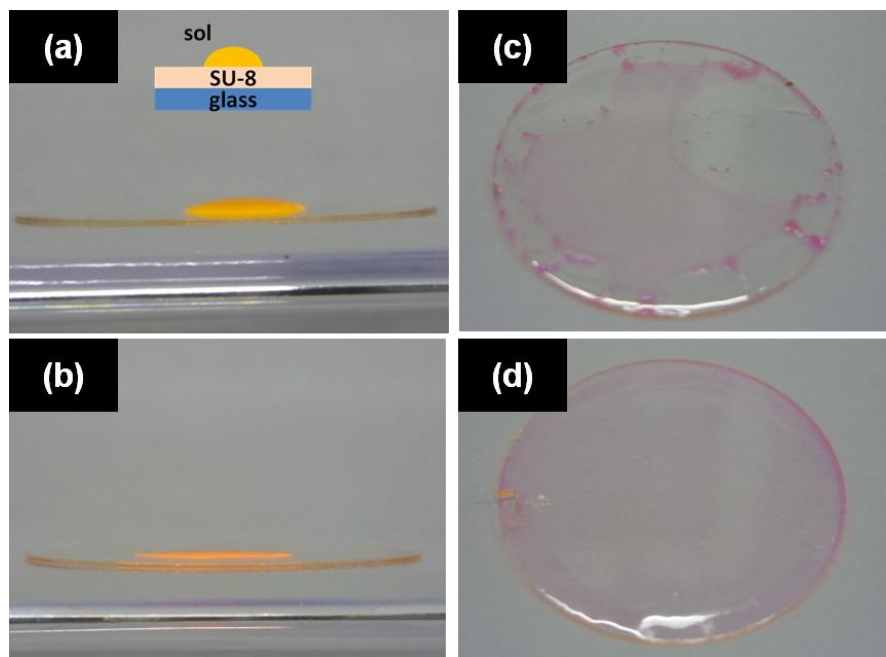
Figure 1. (a) (b): Side-view images of the wetting behavior of two different sols prepared in the molar ratio of (a) 1 TMOS: 18 MeOH: 0.001 HCL: 4 H_2O (b) 1 TMOS: 20 EtOH: 0.004 HCL: 5 H_2O:0.10 CTAB.

(c) (d): Images taken after spin coating the each sol used in (a) and (b), respectively.
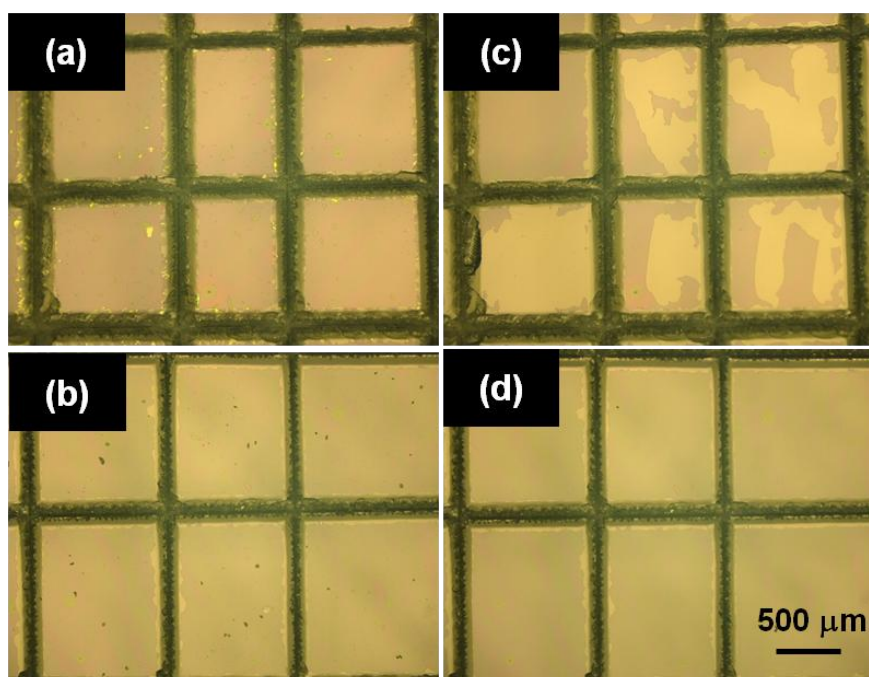
Figure 2. Optical microscope images of cross-cut films (a) (c): without heat treatment and (b) (d): with heat treatment at 100 °C for 1 h and at 150 °C for 1 h. (a) and (b) were taken before tape removal. (c) and (d) were taken after tape removal at the same area as (a) and (b), respectively.
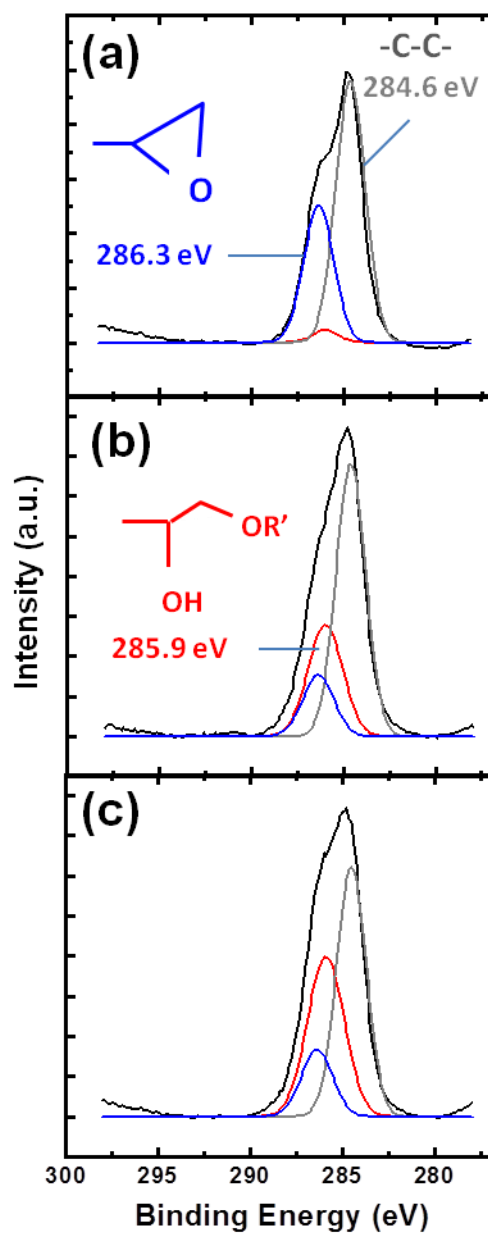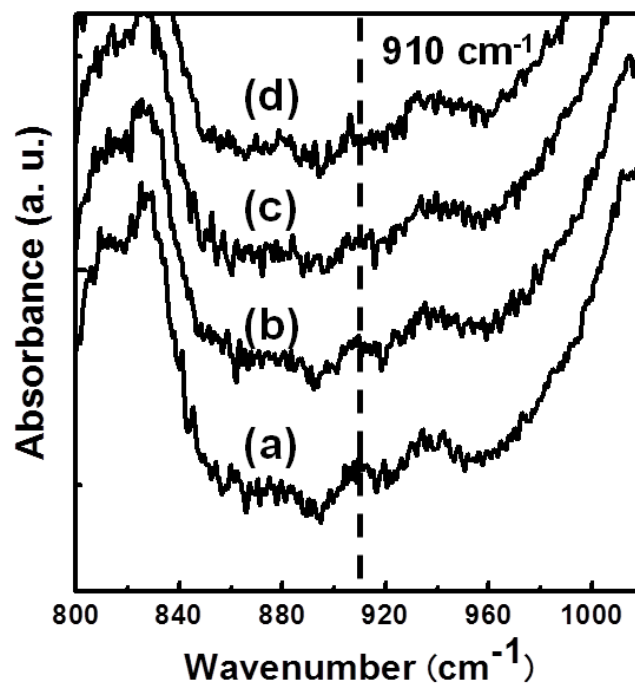
Figure 3. C1s XPS spectra measured on the surface of SU-8 (a) without baking, (b) baked at 100 °C for 2 h   and (c) baked at 100 °C for 2 h and at 150 °C for 2 h.
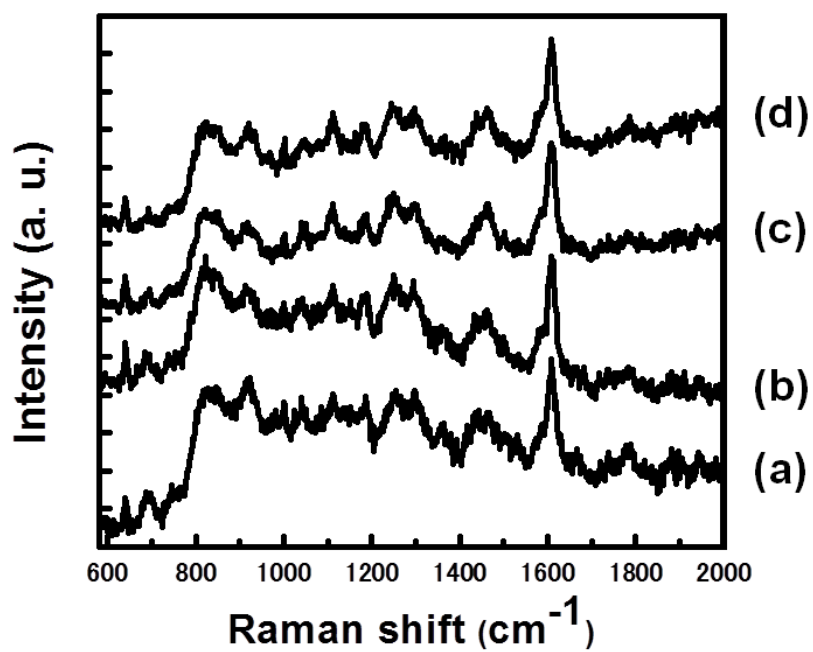
Figure 4. Raman spectra measured on the surface of SU-8
(a) without baking, (b) baked at 100 °C for 1h , (c) baked at 100 °C for 2h and at 150 °C
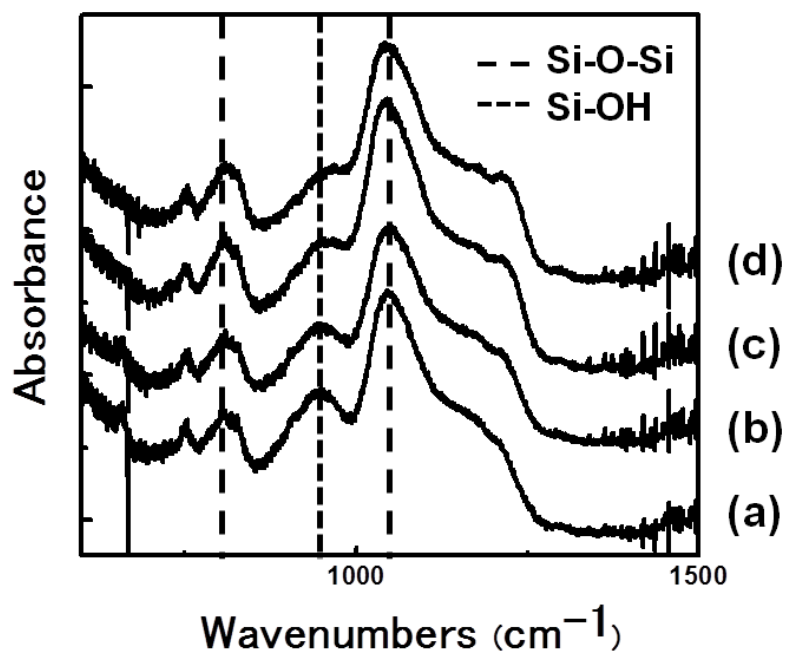for 2h and (d) baked at 100 °C for 2h and at 150 °C for 4h.

Figure 5. FTIR spectra measured on the surface of SU-8 (a) without baking, (b) baked at 100 °C for 1 h , (c) baked at 100 °C for 2 h and at 150 °C for 2 h and (d) baked at 100 °C for 2 h and at 150 °C for 4 h.

Figure 6. FTIR spectra measured on the surface of the SU-8 after coating silica gel film (a) without baking, (b) baked at 100 °C for 1 h , (c) baked at 100 °C for 2 h and at 150 °C for 2 h and (d) baked at 100 °C for 2 h and at 150 °C for 4 h.
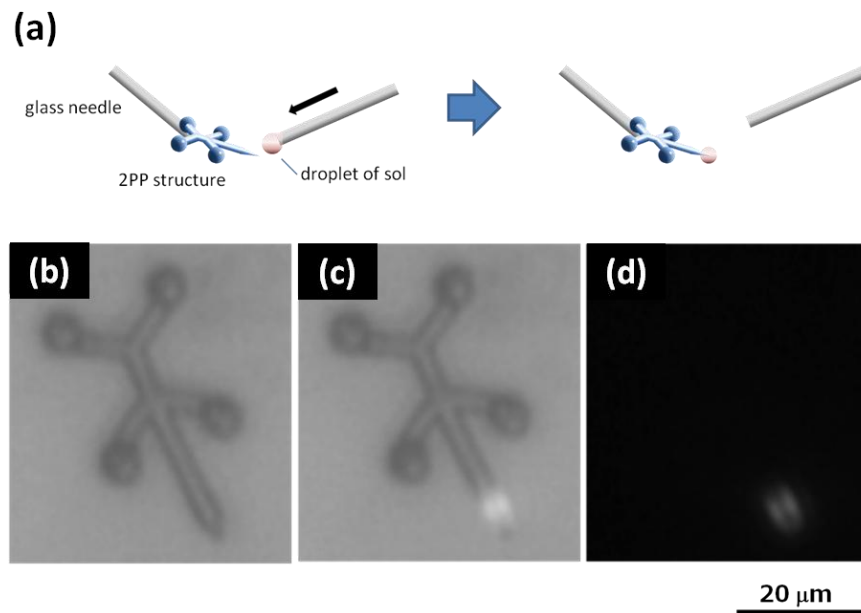
Figure 7. (a) Schematic representation of the procedure to coat microstructures. (b) (c) (d): Optical microscope images of the fabricated structure. (b) was taken under white illumination. (c) and (d) was taken with 532 nm CW laser. (d) was observed with high-pass filter which rejects radiation below 540 nm.
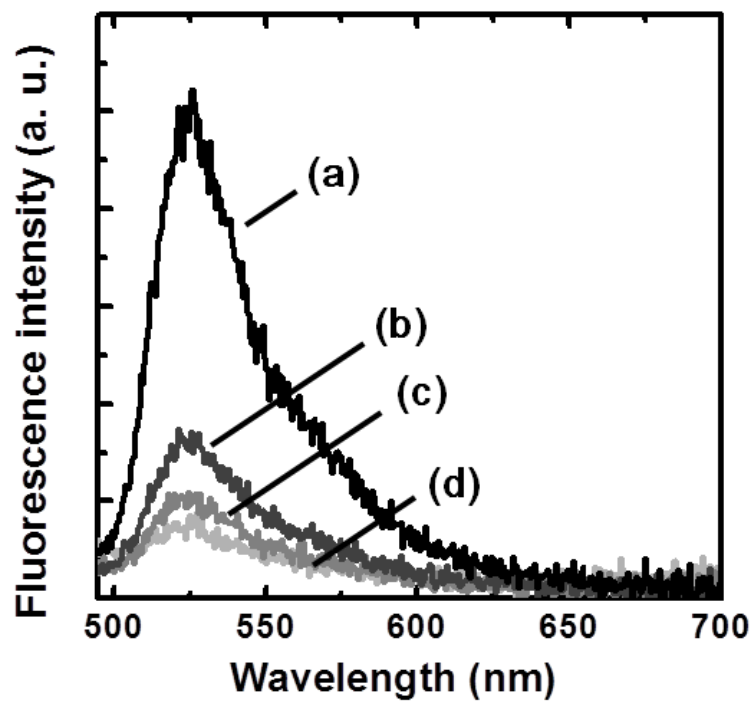
Figure 8. Fluorescence emission spectra of sol-gel film. Each spectrum was measured after immersing film in (a) 10 mM Ca^{2+} solution, (b) 0.1 mM Ca^{2+} solution, (c) 0.001 mM Ca^{2+} solution, and (d) pure water.
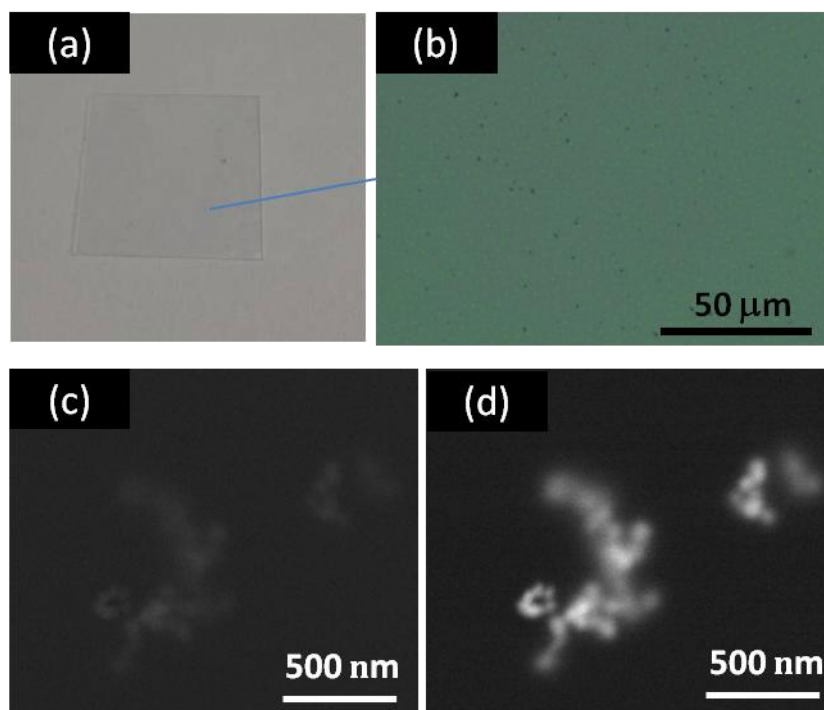
Figure 9. Observation of the film fabricated with gold nanoparticles: (a) optical image, (b) optical microscope image, (c) secondary electron image by FE-SEM, and (d) backscattered electron image, respectively.
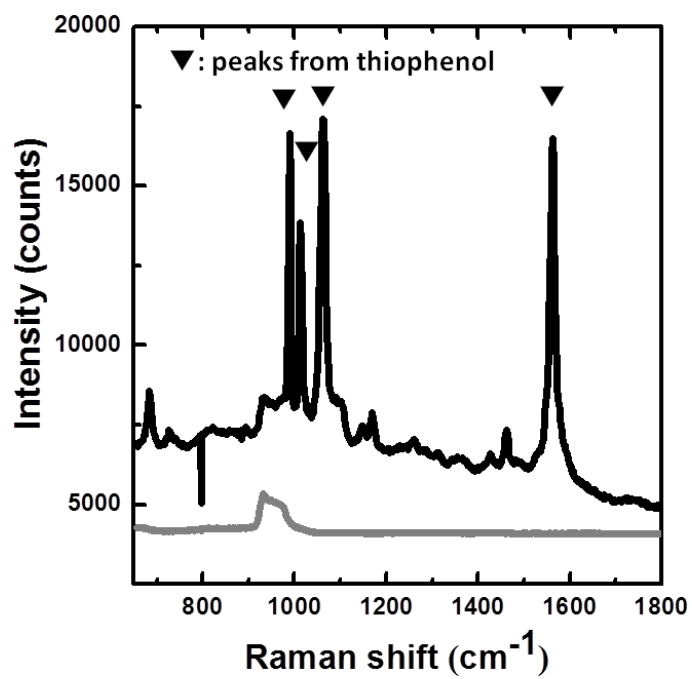
Figure 10. Raman spectra measured on the film with (black line) and without (gray line) gold nanoparticles after immersing them in a dilute ethanol solution of thiophenol.

References

[1]   H Lorenz, M Despont, N Fahrni, N LaBianca, P Renaud and P Vettiger, J. Micromech. Microeng. **7** (1997), 121

[2]   S. Balslev, A. M. Jorgensen, B. Bilenberg, K. B. Mogensen, D. Snakenborg, O. Geschke, J. P. Kutter and A. Kristensen, Lab on a Chip **6** (2006), 213

[3]   A. Sundaramurthy, P. J. Schuck, N. R. Conley, D. P. Fromm, G. S. Kino and W. E. Moerner, Nano Lett. **6** (2006), 355

[4]   J. Carlier, S. Arscott, V. Thomy, J. C. Fourrier, F. Caron, J. C. Camart, C. Druon and P. Tabourier, J. Micromech. Microeng. **14** (2004), 619

[5]   S. Maruo and J. T. Fourkas, Laser & Photon. Rev. **2** (2008), 100

[6]   A. Ovsianikov, A. Ostendorf, B. N. Chichkov, Applied Surface Science **253** (2007), 6599

[7]   L. Kelemen, S. Valkai and P. Ormos, Applied Optics **45** (2006), 2777

[8]   P.J. Rodrigo, L. Kelemen, D. Palima, C.A. Alonzo, P. Ormos and J. Glückstad Optics Express 17 (2009), 6578

[9]   P. L. Stiles, J. A. Dieringer, N. C. Shah and R. P. V. Duyne, Annual Review of Analytical Chemistry **1** (2008), 601

[10]   K. Kneipp, Y. Wang, H. Kneipp, L. T. Perelman, I. Itzkan, R. R. Dasari and M. S. Feld, Phys. Rev. Lett. **78** (1997), 1667

[11]   X. M. Qian and S. M. Nie, Chem. Soc. Rev. **37** (2008), 912

[12]   O. Seitz, M. M. Chehimi, E. C. Deliry, S. Truong, N. Felidj, C. Perruchot, S. J.

Greaves and J. F. Watts, Colloids and Surfaces A: Physicochemical and

Engineering Aspects **218** (2003), 225

[13]   M. V. Cana-mares, J. V. Garcia-Ramos, J. D. Gomez-Varga, C. Domingo, and S.

Sanchez-Cortes, Langmuir **21** (2005), 8546

[14]   A. Kaminska, O. I. Agha, R. J. Forster and T. E. Keyes, Phys. Chem. Chem.

Phys. **10** (2008), 4172

[15]   R. Marie, S. Schmid, A. Johansson, L. Ejsing, M. Nordstrom, D. Hafliger, C.

BV Christensen, A. Boisen and M. Dufva, Biosensors and Bioelectronics **21**

(2006), 1327

[16]   M. Joshi, R. Pinto, V. R. Rao and S. Mukherji, Applied Surface Science **253**

(2007), 3127

[17]   B. L. Aekbote, J. Jacak, G. J. Schütz, E. Csányi, Z. Szegletes, P. Ormos and L.

Kelemen, European Polymer Journal **48** (2012), 1745

[18]   C. Ingrosso, E. Sardella, S. Keller, S. Dohn, M. Striccoli, A. Agostiano, A.

Boisen and M. L. Curri Advanced Materials **22** (2010), 3288

[19]   H. Podbielsk and A. Ulatowska-Jarza, Bulletin of The Polish Academy of

Sciences Technical Sciences **53** (2005), 261

[20]   P. C. A. Jerónimo, A. N. Araújo, M. Conceição and B.S.M. Montenegro, Talanta
        72 (2007), 13

[21]   O. B. Miled, D. Grosso, C. Sanchez and J. Livage, Journal of Physics and
        Chemistry of Solids **65** (2004), 1751

[22]   H. L. Wu, C. H. Chen and M. H. Huang, Chemistry of Materials **21** (2009), 110

[23]   F. Walther, P. Davydovskaya, S. Z̈urcher, M. Kaiser, H. Herberg, A. M. Gigler
        and R. W. Stark, J. Micromech. Microeng. **17** (2007), 524

[24]   D. Lin-Vien, N. B. Colthrup, W.G. Fateley and J. G. Grasselli, *The Handbook of
        Infrared and Raman Characteristic Frequencies of Organic Molecules*,
        Academic Press Inc., San Diego, 1991.

[25]   A. N. Khramov, V. N. Balbyshev, N. N. Voevodin and M. S. Donley, Progress
        in Organic Coatings **47** (2003), 207

[26]   D. Wong, T. L. Tan, P. Lee, R. S. Rawat and A. Patran, Microelectronic
        Engineering **83** (2006), 1912

[27]   S. Keller, G. Blagoi, M. Lillemose, D. Haefliger and A. Boisen, J. Micromech.
        Microeng. **18** (2008), 125020

[28]   G. Blagoi, S. Keller, A. Johansson, A. Boisen and M. Dufva, Applied Surface
        Science **255** (2008), 2896

[29]   F. Peng, L. Lu, H. Sun, Y. Wang, J. Liu and Z. Jiang, Chem. Mater. **17** (2005), 6790

[30]   Y. L. Liu and S. H. Li, Journal of Applied Polymer Science **95** (2005), 1237

4.2 Functionalization of two-photon polymerized SU-8 surface with fluorescent calcium indicator for the use in optical trapping system

4.2.1 Introduction

Optical trapping was first reported by Ashkin [1] in 1970 and has been attracting more and more attention these days especially in biological fields because it enables us to manipulate microscopic objects three-dimensionally in real-time without any mechanical contact with them [2]. The technique generally uses the forces of radiation pressure arising from the momentum of light itself. Among many systems currently developed for optical trapping, our BioPhotonics Workstation (BWS) has some advantages over other systems; it can generate multiple controllable counter-propagating beams to create real-time user-programmable optical traps for stable three-dimensional control and manipulation of a plurality of particles. We have traditionally used the counter-propagating geometry to achieve stable three-dimensional trapping while maintaining a large working distance by using microscope objectives with relatively low numerical apertures. The BWS affords independent control of the counter-propagating beam patterns and we have earlier exploited this to correctly match the corresponding set of counter-propagating beam traps [3]. With this trapping geometry we are currently able to generate around 100 dynamic optical traps using well-separated

objectives, which eliminates the need for high numerical aperture oil or water immersion objectives required in conventional optical tweezers. This generates a large field of view and leaves vital space for integrating other enabling tools for probing or processing the trapped particles, such as linear and nonlinear microscopy or pulsed laser processing.

Optical trapping is usually demonstrated with dielectric spheres and biological samples. But trapping applications extend beyond readily available samples such as custom designed two-photon polymerized (2PP) structures. Two-photon polymerization has emerged as a promising technique for fabrication of three-dimensional structures [4]. In the 2PP process, femtosecond laser pulses induce nonlinear absorption in a highly localized focal volume which leads to three-dimensional micro- or nanoscopic structures. Not only does it enable flexible fabrication of polymer structures, but it also can be applied for fabrication of new micro/nanostructures or advanced photo-excitations which have functions for communicating with other materials. By combining the functionalized 2PP structures with the BWS platform, novel methods for analyzing and/or processing objects can be realized independently and fully decoupled from the counter-propagating trapping geometry.

Considering the potential of the BWS platform in biological applications [5], [6], I were motivated to fabricate 2PP structures functionalized with fluorescent dyes which can act as sensors for specific ions or temperature in biological environments. This kind of optical sensor can be designed by applying conventional techniques for fiber-optic

sensors (optodes) [7], [8], [9]. While using optodes is basically an indirect sensing method and the fiber connection to external devices sometimes prevents flexible approach to analytes, 2PP structures are expected to work more flexibly and make it possible to detect environmental changes directly by monitoring the fluorescence change of the dyes on a trapping system. However, due to the chemically-inert surfaces of the structures obtained using normal epoxy- or acryl-based resins, functionalization of them directly with dye molecules is generally not straightforward. In section 4.1, I demonstrated that functionalization of SU-8 surface can be achieved by utilizing silica xerogel as host matrix to entrap functional materials. In this work, we applied the method to functionalization of 2PP-fabricated microstructures with fluorescent calcium indicator.

One issue when fabricating microscopic objects using 2PP by a single laser beam is that it needs long processing times. The long processing time makes practical application of 2PP difficult. To solve this problem, we utilized a phase modulation technique with a spatial light modulator (SLM) [10]. The technique allows us to split one laser beam into multiple beams by means of computer generated holograms (CGH). Multiple focused beam spots can be created after focusing, depending on the spatial phase modulation. At each beam focus, the resin is photopolymerized through two-photon absorption, which leads to the creation of polymerized materials at multiple positions at the same time. By combining CGH with computer-generated Fresnel lenses, a flexible and fast two-photon three-dimensional (3D) microfabrication can be realized.

4.2.2 Experimental

1. 2PP processing

The experimental setup for 2PP with an SLM is shown in Fig. 11. Amplified Ti: Al_2O_3 femtosecond laser pulses (Mira-Legend, Coherent Inc.) with a pulse duration of about 120 femtoseconds, central wavelength of 800 nm and repetition rate of 1 kHz were used for the process. The laser pulses were reflected on a liquid crystal on silicon SLM (LCOS-SLM, X10468-02, Hamamatsu Photonics K.K.), which had 800×600 square pixels with a pixel pitch of 20 μm and that can provide a reflected beam with an independent phase change of up to 2π at each pixel [11]. The laser pulses reflecting on the SLM then passed through a telescope, which consisted of two concave lenses (magnification of M = 0.3), and were focused inside a pre-baked resin with an oil immersion objective lens (NA = 1.40; Plan Apo VC, Nikon). The resin was prepared by spin-coating SU-8 3035 (NIPPON KAYAKU) on a cover glass substrate and pre-baked at 95 ˚C for 1 h. The substrate was placed on a 3D translation stage and the spatially phase modulated beam was focused at multiple positions inside the resin. The processing of the structures was observed with a CCD camera and back illumination with a red LED lamp, although the resin shows only a slight change after laser irradiations because the refractive index change of SU-8 occurs not in the irradiation process but in the post-baking process. The laser beam power was controlled at 30 mW with a neutral density (ND) filter, and the exposure time for each hologram was

controlled at 30 ms with a mechanical shutter. The translation stage, LCOS-SLM and mechanical shutter were controlled by a personal computer. The CGHs were calculated by a simple iterative-Fourier-transform algorithm (IFTA) in which the optimization are made by setting a non-zero amplitude to the dark pixels as well as adding a dummy area outside the signal area. A calculated CGH with 512×512 pixels was displayed in the central region of the active area of the LCOS-SLM. The 3D processing was performed by simply superimposing phase Fresnel lens onto the CGH, which leads to a focus shift of multiple spots generated by each hologram. By switching these combined CGHs layer by layer, fast 3D processing was achieved.

It should be noted that for the structure to be released from the substrate after developing but not to be washed away, the 3D writing should start from an inside point of the resin and end at an interface point between the glass and the resin.

2. Functionalization

The laser-processed resin was first post-baked at 95 ˚C for 15 min, followed by developing for 15 min in a SU-8 developer (NIPPON KAYAKU) and rinsing with isopropanol. Preparation of sol-gel solution for coating was performed according to the procedure written in the section 4.1; A prehydrolysed solution was prepared by heating an ethanol solution containing tetramethoxysilane (TMOS), water and hydrochloric acid in the following molar ratio: 1 TMOS: 3 EtOH: 5×10-5 HCl: 1 H2O at 100 ˚C for 1 h. Then, cetyltrimethylammonium bromide (CTAB) was dissolved in ethanol and added to

93

the prehydrolysed solution together with an additional amount of water and HCl. The final molar ratio was 1 TMOS: 20 EtOH: 0.004 HCL: 5 H2O: 0.10 CTAB. The final solution was then stirred for four days at room temperature. 1 ml of a dye ethanol solution (0.13 mM) is then mixed with 1 ml of the sol and left under stirring for several hours. A typical dye used in this work was Fluo-5N (Invitrogen). Coating of 2PP structures were performed by spin-coating the resulting solution on the glass substrate with the structures and then the coated structures were gently released from the substrate by a glass needle and dried in air at room temperature. Before use, the coated structures and films were placed in pure water to remove excess and unbound dyes.

3. Analysis

An FE-SEM (JSM6700F, JEOL) and a Raman microspectrometer (Nanofinder30, Tokyo Instruments; wavelength=633 nm, NA=0.6) was used to investigate and analyze the 2PP fabricated structures. The response of the sol-gel coated structures was observed using a fluorescence microscope with excitation at 490 nm. The fluorescence measurement was performed by first immersing the structures or the film into solutions with various concentrations of calcium ions for 10 minutes and then drying them in air for a few minutes.

4.2.3 Results and Discussions

Figure 12 shows an SEM image of the fabricated structures. Since I used 18 holograms in total for each structure, laser processing for each structure was finished within 1 s. Although the processing can be finished much faster than that of

conventional scanning system, the fabricated structures are not smooth and sometimes randomly rough because of the inhomogeneous nature of laser spots created by the SLM and the constraint on spacing between spots imposed by the discrete Fourier transform procedure. However, considering long processing times of conventional 2PP systems, I believe that our multi-focus approach using LCOS-SLM is acceptable when the smoothness and fineness of the structures are not necessarily required. Introducing additional algorithms such as optimal-rotation-angle method would improve the uniformity of the spots [12], [13], and the spatial configuration of the focus spots would also be optimized by using the method reported by Bengtsson et al. [14]. The poor quality of the structures might also be due to the high repetition rate of the femtosecond laser, i.e., the high energy of single pulses, which possibly causes boiling or destroying of the resin. We need to investigate these points further in future works.

Figure 13 shows fluorescence microscope images of a 2PP structure with sol-gel coating. These images were captured in the same optical condition before (a) and after (b) immersing it in a 10 mM solution of calcium ions. We can clearly see the difference which arises from the response of the entrapped calcium indicators. The sol-gel matrix contained only one dye in this work, but multiple dyes can also be combined in a single matrix, so that a reference standard can be used to minimize possible errors. Additionally, it is potentially possible to entrap any dye inside the matrix. Metal nanoparticles, quantum dots and even enzymes can also be entrapped. By introducing

these structures on the BWS platform, a real-time and flexible measurement of biologically important ions and temperature would be realized.

4.2.4 Conclusion

I used 2PP processing and surface modification to fabricate functionalized microstructures which can act as sensors for calcium ion. To speed up the 2PP processing, I utilized phase modulation technique with a SLM. Although the processing can be finished much faster than that of conventional scanning system, it turns out that the fabricated structures are rough because of the inhomogeneous nature of laser spots created by the SLM and the constraint on spacing between spots imposed by the discrete Fourier transform procedure. Functionalization of the structures was performed by coating them with silica-based sol-gel materials which contain fluorescent calcium indicator inside. The fluorescence measurements showed that entrapped dyes remain sensitive in the sol-gel matrix, indicating the potential of the coated structures as sensors in biological environments.
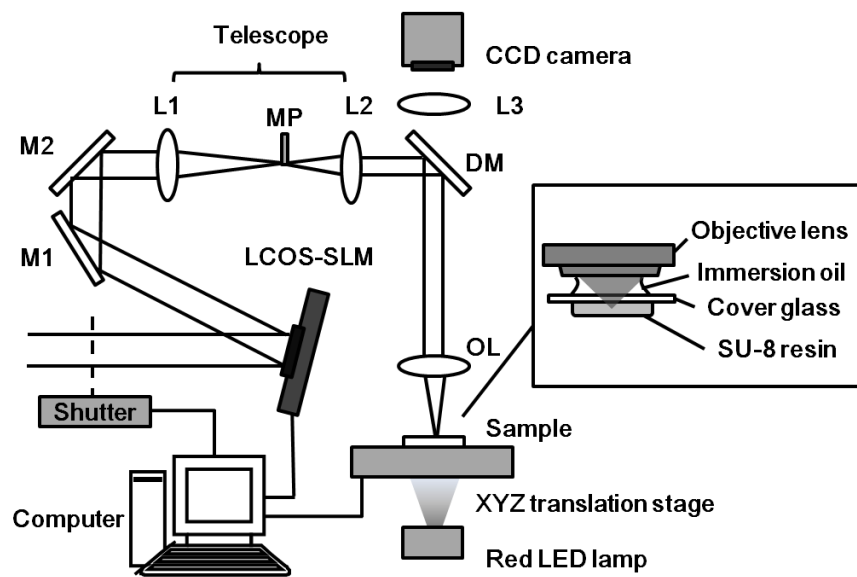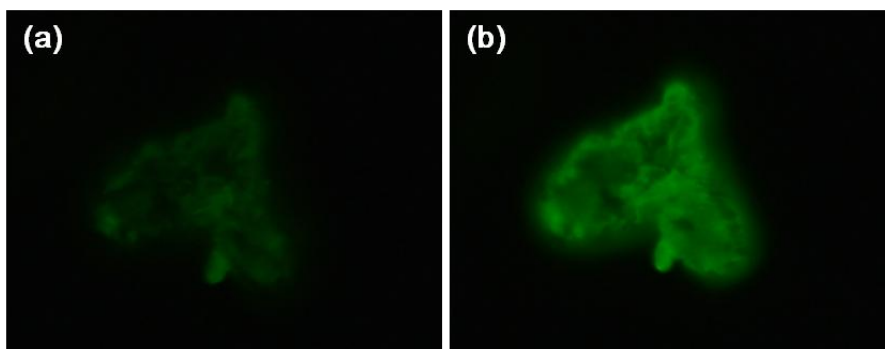
Figure 11. Experimental setup for 2PP fabrication with an SLM . M1, M2: dielectric mirrors;

L1: a lens of f = 500 mm; L2: a lens of f = 150 mm; DM: a dichroic mirror which reflects   light of 750-850 nm; OL: an objective lens; MP: a metal plate.
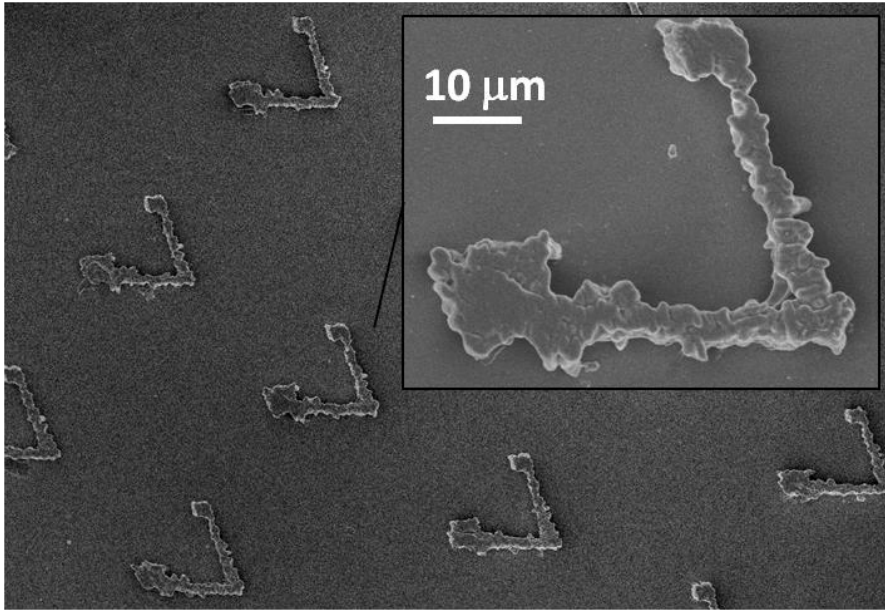
Figure 12. SEM images of the obtained 2PP structures

Figure 13. Fluorescence images with excitation at 490 nm: (a) sol-gel coated structure in water   and (b) in 10 mM Ca^{2+} solution. The structure were immersed in the respective solution for 10 minutes and dried before measurements.

References

[1]   A. Ashkin, Phys. Rev. Lett. 24 (1970), 156

[2]   J. Glückstad, Nature Materials 3 (2004), 9

[3]   P. J. Rodrigo, L. Kelemen, D. Palima, C. A. Alonzo, P. Ormos, and J. Glückstad, Opt. Express **17** (2009), 6578

[4]   S. Kawata, H. B. Sun, T. Tanaka and K. Takada, Nature **412** (2001), 697

[5]   E. Papagiakoumou, F. Anselmi, A. Begue, V. de Sars, J. Glückstad, E. Isacoff and V. Emiliani, Nature Methods **7** (2010), 848

[6]   H.U. Ulriksen, J. Thøgersen, S. Keiding, I. P.-Nielsen, J. Dam, D. Z. Palima, H. Stapelfeldt and J. Glückstad, J. Europ. Opt. Soc. Rap. Public. **3** (2008), 08034

[7]   S. L. R. Barke, B. A. Thorsrud and R. Kopelman, R., Anal. Chem. **70** (1998), 100

[8]   W. E. Morf, K. Seiler, B. Rusterholz and W. Simon, Anal. Chem. **62** (1990), 738

[9]   B. D. MacCraith, C. McDonagh, A. K. Mcevoy, T. Butle, G. OKeeffe and V. Murphy, J. Sol–Gel Sci. Technol. **8** (1997), 1053

[10]   M. Sakakura, T. Sawano, Y. Shimotsuma, K. Miura and K. Hirao, Jpn. J. Appl. Phys. **48** (2009), 126507

[11]   T. Inoue, H. Tanaka, N. Fukuchi, M. Takumi, N. Matsumoto, T. Hara, N. Yoshida, Y. Igasaki and Y. Kobayashi, Proc. SPIE Y**11** (2007), 6487

[12]   J. Bengtsson, Appl. Opt. **33** (1994), 6879

[13]   H. Takahashi, S. Hasegawa and Y. Hayasaki, Appl. Opt. **46** (2007), 5917

[14]   D. Engström, A. Frank, J. Backsten, M. Goksör and J. Bengtsson, Opt. Express **17** (2009), 9989

List of Publications

Chaper 1

"Selective growth of gold nanoparticles on FIB-induced amorphous phase of Si substrate",
<u>Tomoyo Matsuoka,</u> Masayuki Nishi, Yasuhiko Shimotsuma, Kiyotaka Miura and Kazuyuki Hirao
Journal of the Ceramic Society of Japan, Vol. 118 pp. 575-578 (2010)

Chapter 2

" Gold patterning on silicon substrate using femtosecond laser",
<u>Tomoyo Matsuoka,</u> Masayuki Nishi, Masaaki Sakakura, Yasuhiko Shimotsuma, Kiyotaka Miura and Kazuyuki Hirao
To be submitted for Optical Express

Chapter 3

" Selective Growth and SERS Property of Gold Nanoparticles on Amorphized Silicon Surface",
<u>Tomoyo Matsuoka,</u> Masayuki Nishi, Masaaki Sakakura, Yasuhiko Shimotsuma, Kiyotaka Miura and Kazuyuki Hirao
IOP Conference Series: Materials Science and Engineering, Vol. 18, p. 052007 (2011)

" Facile and flexible fabrication method for SERS-active substrate using selective metal growth on silicon"
<u>Tomoyo Matsuoka,</u> Masayuki Nishi, Yasuhiko Shimotsuma, Kiyotaka Miura and Kazuyuki Hirao
To be submitted for Applied Physics A

" Localized control of light–matter interactions by using nanoscale asymmetric TiO_2"
Shifeng Zhou, <u>Tomoyo Matsuoka</u>, Yasuhiko Shimotsuma, Masaaki Sakakura, Masayuki
Nishi, Zhanglian Hong, Jianrong Qiu, Kazuyuki Hirao and Kiyotaka Miura
Nanotechnology, Vol. 23, p.465704 (2012)

Chapter 4

" Functionalized 2PP structures for the BioPhotonics Workstation"
<u>Tomoyo Matsuoka,</u> Masayuki Nishi, Masaaki Sakakura, Kiyotaka Miura, Kazuyuki
Hirao, Darwin Palima, Sandeep Tauro, Andrew Bañas and Jesper Glückstad
SPIE, Vol. 7950, p. 79500Q (2011)

"Funtionalization of SU-8 by sol-gel immobilization technique"
<u>Tomoyo Matsuoka,</u> Masayuki Nishi, Yasuhiko Shimotsuma, Kiyotaka Miura and
Kazuyuki Hirao
To be submitted for Lab on a Chip

Acknowledgment

The present thesis has been carried out under the direction of Professor Kazuyuki Hirao at Graduate School of Engineering , Kyoto University.

First of all, the author genuinely express her gratitude to Professor Kazuyuki Hirao for his continuous encouragement and valuable advice all through the duration of the present work. The author is also profoundly grateful to Professor Kiyotaka Miura and Professor Jesper Gluckstad for the guidance and discussion in preparation of the present thesis.

The author is greatly indebted to Assistant professor Masayuki Nishi. His instructive advices have been essential to the consistent progress of my research and the guidance has been thoughtful and brushed up my research.

The author also sincerely appreciates Associate professor Yasuhiko Shimotsuma, Associate professor Masaaki Sakakura and Dr. Shingo Kanehira for helpful suggestion and discussion.

The author expresses her sincere thanks to all the students and researchers in both Hirao laboratory and Miura laboratory.

Finally, the author would like to express her profound appreciation to her husband, Yasushi Matsuoka, her mother, brother and sister for their understanding, supports and hearty encouragements.

<div align="right">Tomoyo Matsuoka</div>